Advances in Engineering Software 217 (2026) 104145

Contents lists available at ScienceDirect

Advances in Engineering Software

journal homepage: www.elsevier.com/locate/advengsoft

Machine learning-driven capacity design and embodied carbon reduction optimization in composite reduced web section (RWS) connections

Mohamed Rabie [a], Fahad Falah Almutairi [b], Konstantinos Daniel Tsavdaridis [c,*], Ibrahim G. Shaaban [a]

[a] School of Computing and Engineering, University of West London, St Mary's Road, Ealing W5 5RF, London, UK
[b] Department of Civil & Architectural Engineering, College of Engineering, International University of Science and Technology, Kuwait
[c] Department of Engineering, School of Science & Technology, City St George's, University of London, Northampton Square, EC1V 0HB London, UK

ARTICLE INFO

Keywords:
Reduced Web Section (RWS) Connections
Ensemble machine learning
Multi-objective optimisation
Sustainable structural design
Embodied carbon

ABSTRACT

A gap in current predictive modelling approaches limits the ability to accurately assess the mechanical, durability performance and sustainability metrics of Reduced Web Section (RWS) connections. This paper addresses this gap by developing an ensemble machine learning (ML) framework combined with multi-objective optimisation, enabling the efficient prediction of seven key mechanical and ductility properties alongside total embodied carbon (EC) reduction. Three ensemble ML models—Extra Trees Regressor (ETR), Gradient Tree Boosting (GTBR), and Extreme Gradient Boosting (XGBoost)—were evaluated, with XGBoost demonstrating superior generalization across most outputs. Additionally, Shapley Additive Explanations (SHAP) analysis was conducted to identify the most influential design parameters, improving model interpretability. The multi-objective optimisation performed using NSGA-II, generated Pareto-optimal solutions, highlighting trade-offs between structural performance and sustainability considerations. The findings reveal that cross-sectional properties, material stiffness, and connection type significantly impact RWS performance, and optimising these parameters can lead to improved ductility, moment capacity, and reduced environmental impact. To enhance practical applicability, a user-friendly interface was developed and deployed via Hugging Face, allowing users to test the results, make predictions and retrieve optimal design parameters based on the nearest Pareto-optimal solutions. The results of this paper demonstrate that ensemble ML methods, coupled with optimisation and explainability tools, provide a robust framework for advancing RWS connection design, ensuring both seismic resilience and sustainability in structural engineering.

1. Introduction

There has been successful research in developing fuse strategies that cluster deformation demand away from the column face, well within the beam [1–3]. However, this approach involves the extensive intervention of the column and provision of stocky supplemental plates on flanges and the web, making retrofitting of structures complex, particularly if they were not designed with full consideration of capacity design principles. On other hand, the escalating climate crisis necessitates a re-evaluation of civil engineering practices, as steel production generates 1–3 t of carbon emissions per metric ton [4] and UK structural concrete emits approximately 250 kgeCO_2 equivalent per cubic meter [5]. Reduced Web Section (RWS) connection emerges as a promising solution in this context, acting as a ductile fuse and economically addressing the limitations of traditional connections. These rely on perforations made on the beam's web rather than flange trimming or the use of supplemental plates to increase moment capacity at the column's face. In particular, it is easier to cut through webs than remove floors to intervene on dysfunctional beam flanges.

Absorbing seismic demand energy within the RWS connections localise failures, through fostering a Vierendeel mechanism that enhances seismic performance and mitigates asymmetric yield effects [6–11]. Such mechanism ensures that critical gravity load-bearing columns remain protected from extensive plastic deformation and potential structural failure during seismic events. Such connection simplifies manufacturing and retrofitting and helps prevent out-of-plane instability. These practical implications underscore the importance of our research in the field of seismic engineering.

The absence of a systematic design methodology to control the

* Corresponding author.
E-mail address: konstantinos.tsavdaridis@city.ac.uk (K.D. Tsavdaridis).

https://doi.org/10.1016/j.advengsoft.2026.104145
Received 13 April 2025; Received in revised form 26 January 2026; Accepted 2 March 2026
Available online 7 March 2026

List of Notations

d_o	Web opening diameter.
S_e	End-distance from column/connection face to centreline of web opening.
h_c	Column section height/depth
b_{cf}	Steel column flange width
t_{cf}	Steel column flange thickness
t_{cw}	Steel column web thickness
L_c	Column length (distance between supports or loading points)
A_a	Beam section cross-sectional area.
h_b	Steel beam depth
b_{bf}	Steel beam flange width
t_{bf}	Steel beam flange thickness
t_{bw}	Steel beam web thickness
L_b	Beam span
r_y	Radius of gyration of steel beam
f_{ync}	Column nominal yield stress
E_{column}	Column modulus of elasticity
f_{ynb}	Beam nominal yield stress
E_{beam}	Beam modulus of elasticity
f_c	Concrete measured characteristic compressive strength.

seismic performance of RWS connections through key geometric parameters has driven significant efforts over the past decade to develop robust guidance, numerical models, and acceptance criteria [6,7,10,12–17]. These studies have indicated that the response of structural moment frames (SMFs) can be assessed by evaluating the extent of damage it undergoes during a non-linear analysis, which mimics realistic seismic conditions. By altering the geometry of the RWS (i.e., web opening size and location) connections can influence its seismic response, providing opportunities to enhance the overall performance and resilience of the SMFs [8,18–21]. Still, no comprehensive analytical, mechanical or empirical model are currently available that account for all the design parameters affecting the non-linear response of RWS connections. This complexity arises from the multiple deformable components within the steel-concrete composite joint (e.g., column, connection, and beam) accurate prediction using simple regression analysis which is not sufficient to capture such complexity. The ability of machine learning to address this complex issue holds significant promise, offering potential computational techniques that could synthesise complex multi-parameter interactions and develop more predictive, comprehensive models in structural engineering field [22–24].

The application of ensemble machine learning (ML) models in predicting the properties of RWS connections presents a significant advancement in structural engineering applications. Traditional empirical or numerical approaches often struggle to generalize across varying geometric and material properties, particularly due to the nonlinear interactions between multiple design parameters such as web opening size, location, and section stiffness [25–27]. Ensemble ML techniques, including bagging and boosting methods, have proven to be highly effective in structural performance prediction due to their ability to capture complex dependencies, reduce variance, and improve generalization accuracy [28–31]. Specifically, ensemble models such as Gradient Boosting, and Extreme Gradient Boosting (XGBoost) leverage multiple weak learners to construct a more robust predictive framework, mitigating overfitting and enhancing model stability across diverse datasets. Studies have shown that ensemble-based approaches outperform single-model regression techniques in predicting structural behavior, including seismic performance, material strength, and damage assessment [32,33]. Given the highly nonlinear nature of RWS connections, utilizing ensemble ML provides a computationally efficient alternative to iterative numerical simulations, enabling rapid design exploration and performance optimization.

Moreover, recent advancements in ML interpretability techniques, such as Shapley Additive Explanations (SHAP) and permutation feature importance, further reinforce the applicability of ensemble methods in structural engineering. These techniques allow for transparent decision-making by identifying the most influential parameters governing RWS connection behavior, thus bridging the gap between data-driven modelling and engineering intuition [34,35]. Unlike black-box deep learning models, ensemble-based approaches maintain a balance between predictive power and interpretability, making them particularly suitable for engineering applications where explainability is crucial [36]. Furthermore, one of the key advantages of RWS connections is their sustainability, as they require less steel compared to conventional connections, reducing material consumption and overall embodied carbon. This makes RWS connections particularly valuable in the context of sustainable structural design, where optimizing material efficiency without compromising structural integrity and seismic performance is a priority [37]. Integrating RWS connections into the capacity design framework and multi-objective optimization process is essential, yet research in this area remains limited. Optimizing RWS connections not only enhances structural durability and performance but also contributes to sustainability efforts by reducing material consumption and embodied carbon. This aligns with global initiatives aimed at minimizing the environmental impact of the construction industry while improving structural resilience [38]. Given these advantages, this study aims to develop an ensemble ML-driven framework to predict the mechanical properties and sustainability performance of RWS connections, leveraging multi-objective optimisation to balance mechanical, ductility performance and embodied carbon reduction. By integrating machine learning, optimisation, and explainability tools, this research aims to provide a systematic data-driven approach for the design and performance assessment of RWS connections, addressing the current knowledge gaps in empirical and numerical modelling approaches as illustrated in Fig. 1.

2. Research significance

Despite extensive research on RWS connections, a significant gap remains in the development of systematic, data-driven methodologies for predicting their mechanical performance and sustainability metrics. Existing studies primarily rely on empirical models, numerical simulations, or experimental testing, which, while valuable, are often computationally expensive, time-consuming, and limited in generalizability across different design configurations. Furthermore, current analytical and numerical approaches struggle to account for the complex nonlinear interactions between key geometric parameters, material properties, and connection behavior under seismic loading. While some studies have attempted to optimize RWS designs, there is a lack of comprehensive multi-objective optimisation frameworks that simultaneously balance seismic performance and environmental impact. Additionally, machine learning applications in RWS design remain underexplored, with most prior work in structural engineering focusing on material property prediction or damage assessment rather than holistic connection performance modelling. The absence of interpretable, ensemble-based machine learning models that can effectively predict multiple mechanical properties while providing insights into feature importance further underscores the need for this research. By addressing these limitations, this study fills a critical gap in the literature by developing an ensemble ML-driven predictive framework combined with multi-objective optimisation, enabling more accurate, efficient, and sustainable design strategies for RWS connections.

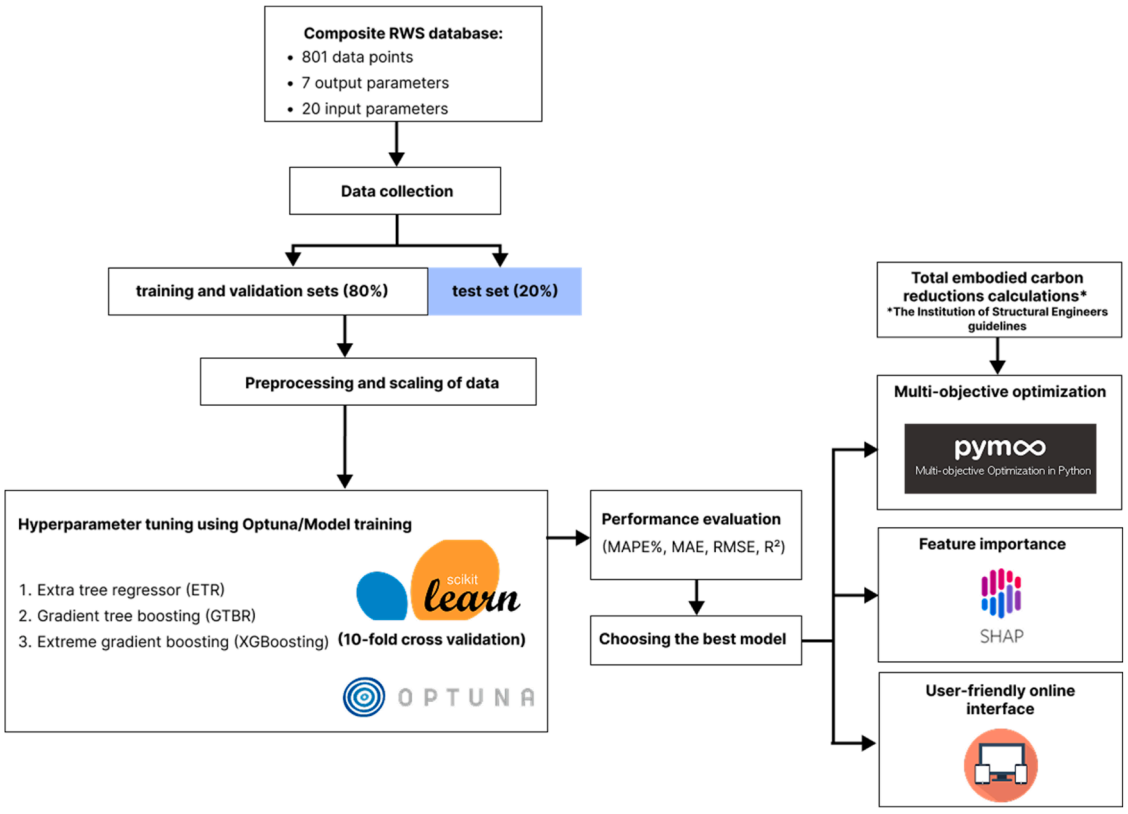

Fig. 1. Flowchart of the ML process with the user-friendly interface.

3. Methodology

3.1. Data description

A comprehensive database of RWS connections has been assembled, encompassing data from 16 test and finite element (FE) programmes as illustrated in Table 1, Fig. 2 and Fig. 3. For each test specimen, 150 parameters were systematically extracted and tabulated to provide a complete characterization. These parameters include the primary attributes of the test programme, geometric properties, material characteristics, and response variables. In this study, the selected parameters, refined from the initial set based on the most relevant predictors, are tabulated in Table 2. The database was standardised using SI units to ensure consistency and is available online as mentioned in the data availability statement.

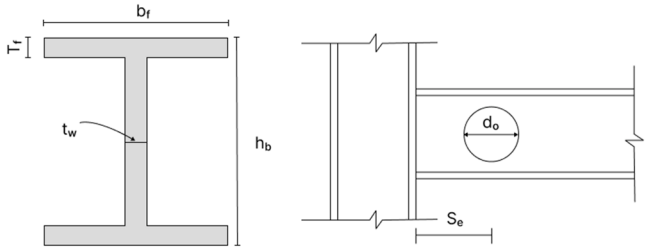

Fig. 2. RWS connection beam and opening parameters.

Table 1
Summary breakdown of the collected RWS database.

Ref.	Total tested specimens/FE models	Study	Connection	Column Section	Beam Section
Guo et al. (2011) [39]	14	FE	Welded	H500 × 350 × 14 × 18	H600 × 250 × 10 × 14
Li et al., (2011) [40]	4	Exp	Welded	H450 × 300 × 12 × 16	H400 × 200 × 8 × 12
Tsavdaridis et al., (2014) [13]	10	FE	Welded	HEB 300	HEA 240
Tsavdaridis and Papadopoulos, (2016) [41]	2	FE	BEEP-3-R	HEB 160	IPE 300
Shin et al., (2017) [42]	2	Exp	WUF-B	W14×145	W12×50 W16×40
Erfani and Akrami, (2017) [7]	1	FE	Welded	HB500×200×10×16	HB414×405×18×28
Shaheen et al., (2018) [19]	13	FE	PN	HB428×407×20×35	HB700×300×13×24
Zhang et al., (2019) [43]	5	FE & Exp	Welded	HW250×250×9×14	HN300×150×6.5×9
Boushehri et al., (2019) [18]	148	FE	Welded	HEB 300, 450, 500, 650	IPE 330, 450, 500, 600
Nazaralizadeh et al., (2020) [11]	1	FE	BEEP-4-R	HEB 200	IPE 270
Tsavdaridis et al., (2021) [10]	1	Exp	BEEP-3-R	UC 203×203×71	UB 305×127×48
Xu et al., (2022) [44]	6	Exp	Welded	HW250×250×9×14	HN300×150×6.5×9
Almutairi et al., (2023) [20]	48	FE	BEEP-4-R	HEB 320	IPE 300
Almutairi et al. (2024) [8]	3	Exp	BEEP-4-R	UC 305×305×198	UB 305×165×54
Almutairi and Tsavdaridis, (2024) [6]	543	FE	BEEP-4-R	310 UC 158	310 UB 32.0

Note: # = number. FE = Finite element analysis. Exp. experimental test. BEEP-3-R and 4-R = bolted extended end-plate with 3 rows and 4 rows, respectively. WUF-B = welded unreinforced flange-bolted web. PN = pre-Northridge.

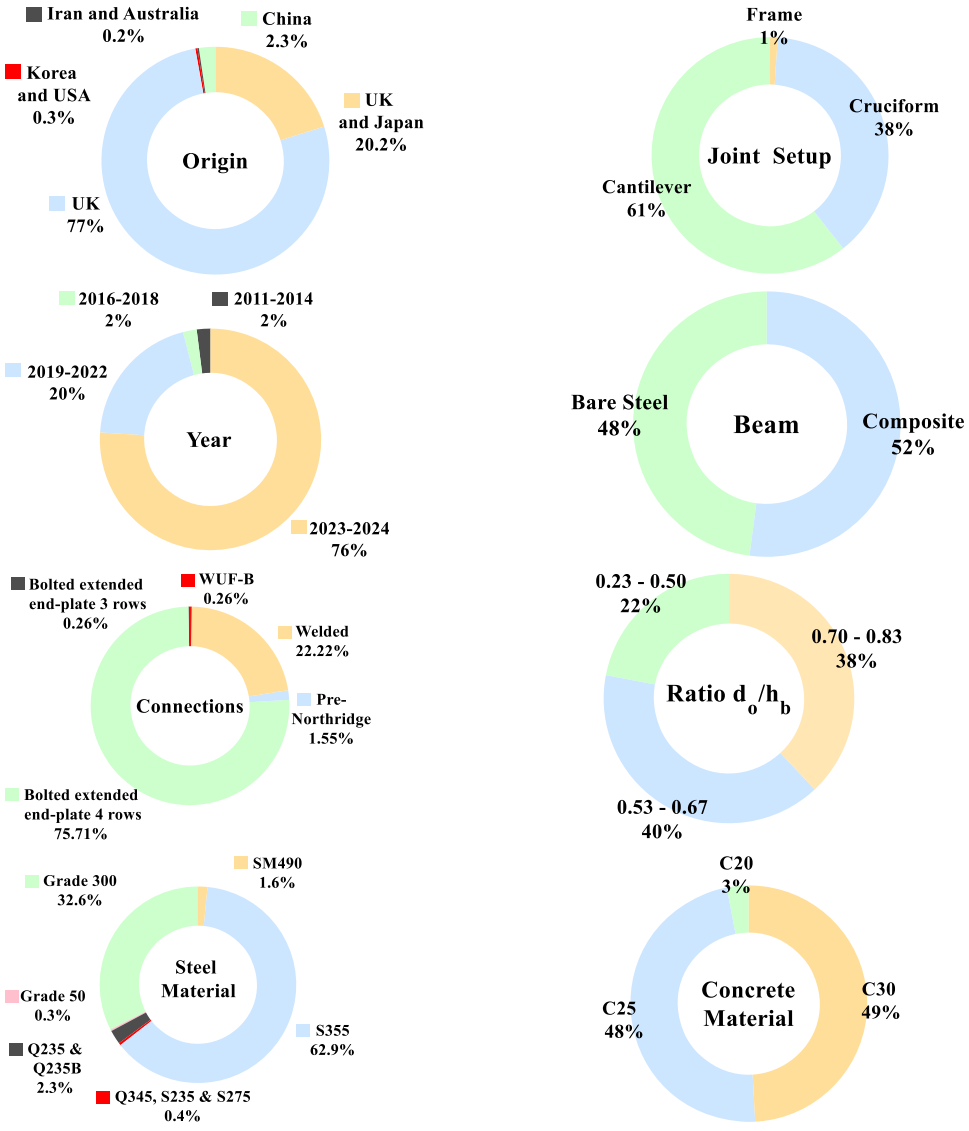

Fig. 3. Disaggregated description of assembled RWS databases.

This database encompasses both bare steel and composite RWS connections, as well as benchmarked solid webbed-beam connections. The database accounts for different types of test setups, namely, cantilever, cruciform and frame arrangements, with load and/or displacement is applied at the beam, or the column ends. Data for both welded and bolted extended end-plate connections are included, featuring configurations with three or four rows of bolts. Additionally, the database captures variations in steel and concrete cross-sectional geometries, nominal and measured material properties, from specifications of different countries.

The database was compiled and analysed as detailed in Almutairi and Tsavdaridis (2020) [6]. The selection criteria were defined to ensure a robust and relevant dataset for both non-seismic and seismic design applications, focusing on: (1) connections with a single circular web opening to standardize geometric analysis; (2) inclusion of detailed experimental or FE data to ensure reliability; and (3) coverage of monotonic and cyclic loading conditions, with monotonic loading specifically added to evaluate non-seismic performance and cyclic loading to assess seismic resilience through metrics such as ductility, moment capacity, and energy dissipation. through metrics such as ductility, moment capacity, and energy dissipation.

The descriptive statistics of the dataset, which consists of 801 RWS connection samples is shown in Table 2, covering a range of geometric, material, and mechanical properties. The dataset includes five connection types, with the Bolted Extended End-Plate (4 rows) configuration being the most common, followed by the Welded Connection, Pre-Northridge, Bolted Extended End-Plate (3 rows), and WUF-B. The geometric parameters show considerable variation, with web opening diameter (d_o) ranging from 0 to 525 mm, End-distance of a web opening (S_e) varying from 0 to 1675 mm (mean = 353.74 mm), and column height (h_c) ranging between 160 mm and 650 mm (mean = 362.12 mm). The flange thickness (t_{bf}) ranges from 8 mm to 28 mm, while the web thickness (t_{bw}) spans from 6 mm to 18 mm, influencing the capacity metrics of the RWS connections. The material properties also exhibit variability, with column yield strength (f_{ynC}) and beam yield strength (f_{ynB}) averaging 338.25 MPa and 336.69 MPa, respectively, while concrete compressive strength (f_c) varies widely from 0 to 38.08 MPa. While all geometric descriptors of the RWS perforation are treated as continuous inputs, the ensemble framework exclusively utilizes one-hot encoding for the categorical connection types to effectively distinguish between the discrete structural topologies.

In total, the database comprises 801 test specimens and FE models of RWS connections, including 20 benchmarked solid webbed-beam counterparts. Despite its extensive scope, a small number of

Table 2
Descriptive statistics of the dataset.

Parameters	Mean	Standard deviation	Minimum	Maximum	Count
Connection Bolted extended end-plate (3 rows)	-	-	-	-	3
Connection Bolted extended end-plate (4 rows)	-	-	-	-	595
Connection Pre-Northridge	-	-	-	-	13
Connection WUF-B	-	-	-	-	2
Connection welded	-	-	-	-	188
d_o	214.58	80.08	0.00	525.00	801.00
S_e	353.74	223.62	0.00	1675.00	801.00
h_c	362.12	82.32	160.00	650.00	801.00
b_{cf}	310.21	19.54	160.00	407.00	801.00
t_{cf}	26.95	4.67	13.00	35.00	801.00
t_{cw}	16.30	2.78	8.00	20.00	801.00
L_c	3284.44	4122.22	1090.00	20,000.00	801.00
A_a	5275.77	2789.89	2649.60	25,068.80	801.00
h_b	346.06	96.52	230.00	700.00	801.00
b_{bf}	169.64	29.72	125.30	405.00	801.00
t_{bf}	12.09	3.53	8.00	28.00	801.00
t_{bw}	7.70	1.72	6.00	18.00	801.00
L_b	4261.46	3785.87	1070.00	20,000.00	801.00
Ry	38.28	6.76	27.40	102.00	801.00
f_{ynC}	338.25	26.81	235.00	413.70	801.00
E(column)	201,617.05	2950.24	193,000.00	210,000.00	801.00
f_{ynB}	336.69	29.59	235.00	372.33	801.00
E(beam)	205,089.93	4426.57	176,500.00	211,331.75	801.00
f_c	17.56	17.41	0.00	38.08	801.00
Yield Moment	327.17	297.20	71.14	2318.55	801.00
Maximum Moment	399.68	343.37	101.76	2488.69	801.00
Ultimate Moment	386.02	347.10	80.10	2488.70	801.00
Dissipated Energy	21.36	10.93	2.49	83.91	801.00
Equivalent Viscous Damping	0.26	0.05	0.06	0.59	801.00
Ductility Under Sagging	3.41	0.84	1.67	7.76	801.00
Ductility Under Hogging	3.71	0.94	1.67	7.76	801.00

experimental and FE programmes were excluded due to insufficient test or modelling details. This database represents a valuable resource for advancing the understanding and development of RWS connections for seismic-resistance structural design.

Although this study does not directly perform seismic simulations or nonlinear FE analysis, it is grounded in the well-established role of RWS connections in seismic-resistant design. RWS detailing is intended to promote ductile behavior through the formation of a Vierendeel mechanism during cyclic loading. The dataset used in this study was compiled from prior test and FE programmes that specifically evaluated the seismic performance of RWS connections. Therefore, while this paper focuses on developing predictive models rather than performing new seismic analyses, the machine learning framework is inherently informed by seismic design considerations. This includes the prediction of cyclic performance indicators such as moment capacity, rotational ductility, and energy dissipation. By abstracting this behavior through ensemble ML models, the study addresses a key gap in current seismic connection design: the lack of accurate, interpretable, and scalable tools for predicting the seismic and sustainability performance of RWS connections.

3.2. Pre-processing of data using correlation matrix

The correlation matrix provides valuable insights into the relationships between input features and output variables in the prediction of RWS connection properties illustrated in Fig. 4. A strong positive correlation is observed among Yield Moment, Maximum Moment, and Ultimate Moment, with correlation coefficients exceeding 0.99, indicating that increasing the flexural strength of the connection generally enhances all three moment capacities. Similarly, Ductility Under Sagging and Ductility Under Hogging exhibit a moderate correlation, suggesting that improving the ductile response in one loading direction can contribute to enhanced deformation capacity in the opposite direction.

Conversely, the correlation between Dissipated Energy and Equivalent Viscous Damping (0.41), while positive, is weaker than expected, implying that energy dissipation is influenced by additional nonlinear mechanisms beyond viscous damping. Several geometric properties, such as flange thickness (t_{bf}), web thickness (t_{bw}), and cross-sectional area (A_a), show high correlations with moment capacities, confirming their significant role in structural resistance. Interestingly, the presence of web openings (d_o) exhibits a negative correlation with moment capacities, reinforcing its weakening effect on flexural strength, while simultaneously showing a moderate positive correlation with ductility parameters, suggesting that RWS connections improve plastic deformation capacity at the expense of moment resistance. Additionally, connection type influences the structural response, with welded connections exhibiting lower correlations with key strength parameters, indicating their distinct behavior compared to bolted alternatives. It is worth noting that feature selection was applied during the data preprocessing stage through the correlation matrix and through manual identification of the most relevant input parameters for RWS connection design. These included key geometric variables and material properties. While certain parameters, such as column length (L_c) and beam span (L_b), exhibited multicollinearity, both were retained due to their fundamental importance in predicting the performance of RWS connections.

These correlation patterns highlight the complex interactions governing RWS connections, emphasizing the importance of using ML to understand this complex interaction and providing accurate predictive modelling. In addition, utilizing multi-objective optimisation in balancing capacity design and sustainability.

3.3. Proposed ML models

This section presents an overview of the ML models employed in this study. Three ensemble ML models were evaluated to develop a robust and accurate predictive framework for the mechanical and ductility properties of composite RWS connections. The study considered seven output variables, namely Yield Moment, Maximum Moment, Ultimate Moment, Equivalent Viscous Damping, Energy Dissipated, Ductility Under Hogging, and Ductility Under Sagging.

The selected models were chosen based on their demonstrated effectiveness in regression tasks in civil engineering applications and their capability to capture complex, non-linear relationships [45–47], which is an essential characteristic when predicting the intricate mechanical and ductility behaviors of composite RWS connections as detailed below. It is worth mentioning that ensemble tree-based methods have also consistently shown superior predictive accuracy and stability compared with single algorithms and artificial neural networks in structural engineering applications [48]. It is worth mentioning that a related methodology was reported in a published work by the first author titled “Glass fibre concrete: Experimental

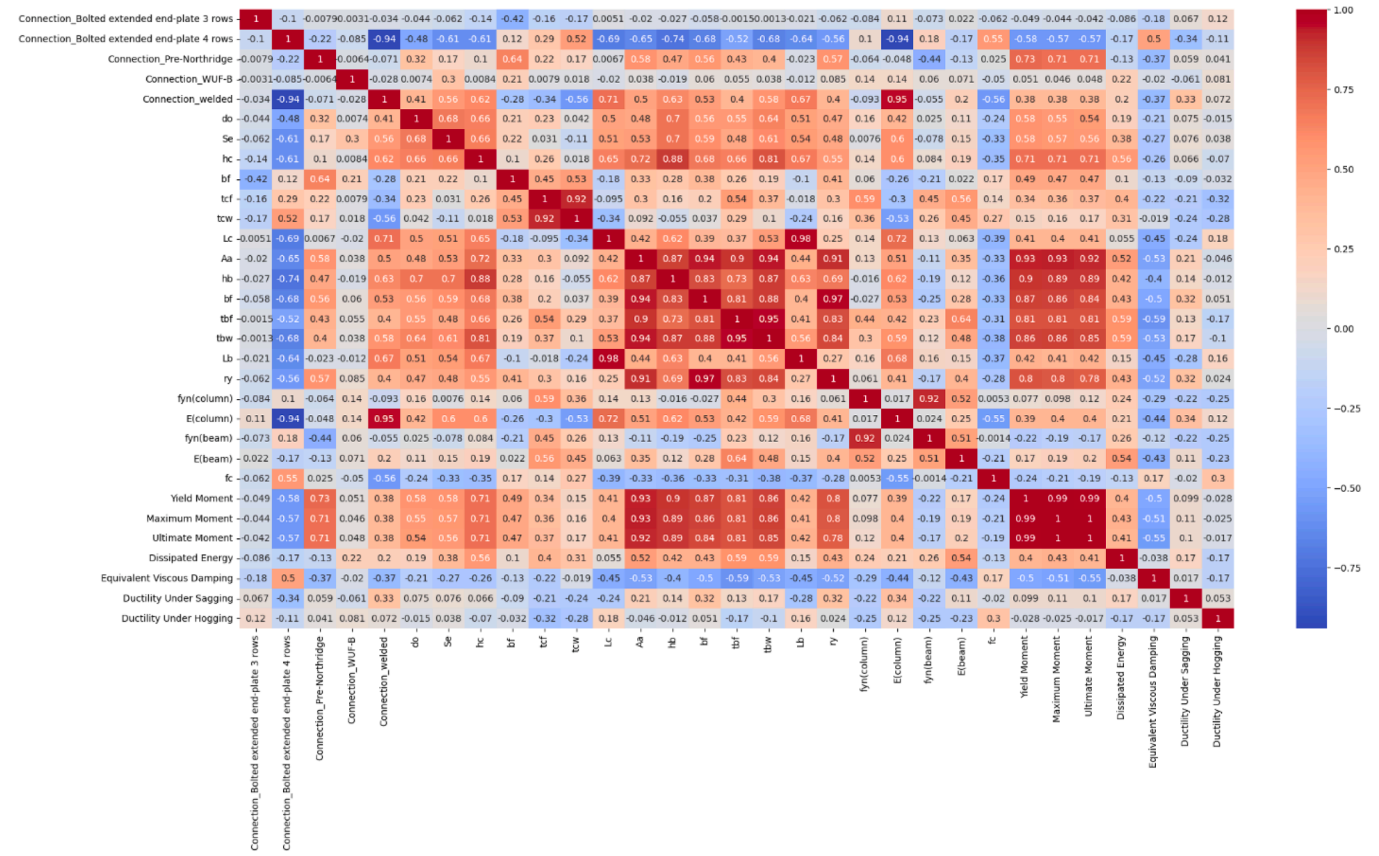

Fig. 4. Correlation matrix between the input and output parameters.

investigation and predictive modeling using advanced machine learning with an interactive online interface."[28,49]. While that study compared both single and ensemble models, the present work focuses exclusively on ensemble algorithms to better capture the complex input-output relationships in RWS connections. In addition, this study incorporates multi-objective optimisation to balance seven mechanical/ductility properties with embodied carbon reduction and uses a more comprehensive dataset of 801 experimental and finite element cases, offering greater predictive robustness and broader design scope.

3.3.1. Extra tree regressor

The Extra Trees Regressor, or Extremely Randomized Trees, is an ensemble-based machine learning method that extends the principles of the Random Forest algorithm by incorporating an additional level of randomness into the tree construction process. Unlike conventional decision tree-based models that optimize split thresholds based on impurity reduction criteria, Extra Trees selects split points completely at random, thereby increasing variance among individual trees while maintaining computational efficiency. The algorithm constructs an ensemble of fully grown decision trees, each trained on the entire dataset rather than using bootstrap resampling, as is the case with Random Forests. At each node, a random subset of features is selected, and for each selected feature, a split threshold is chosen at random. The split that yields the best reduction in variance is then applied to partition the data. This aggressive randomization reduces variance in the final ensemble while slightly increasing bias, leading to a robust and computationally efficient model for regression tasks [50].

Mathematically, the prediction of Extra Trees Regressor follows the general form of an ensemble averaging method. Given a dataset $\mathscr{D} = \{(x_i, y_i)\}_{i=1}^{N}$, where $x_i \in R^d$ represents the feature vector and $y_i \in R$ is the target variable, the prediction for a new input $x^*$is obtained by averaging the predictions of T individual decision trees as shown in Eq.1 :

$$\hat{y}(x) = \frac{1}{T}\sum_{t=1}^{T} f_t(x) \tag{1}$$

where $f_t(x)$ is the prediction from the t-th tree in the ensemble. Each decision tree operates by recursively splitting the feature space using randomly chosen thresholds. At each internal node, a subset $\mathscr{S} \subseteq \{1, \ldots, d\}$ of K features is randomly selected, and a split threshold $s_j$is chosen uniformly at random from the range of values in feature x_j as shown in Eq. 2:

$$s_j \sim U(x_{j,min}, x_{j,max}) \tag{2}$$

$x_{j,min}$and$x_{j,max}$ the minimum and maximum values of feature x_j in the current node. The best feature j^* is then selected by minimizing the weighted variance reduction as shown in Eq. 3:

$$j^* = \underset{j\in\mathscr{S}}{\operatorname{argmin}}\left[\frac{N_L}{N}\mathrm{Var}(Y_L) + \frac{N_R}{N}\mathrm{Var}(Y_R)\right] \tag{3}$$

where Y_L and Y_R are the target values of the left and right child nodes, respectively, and N_L and N_R denote the number of samples in the left and right partitions.

The final ensemble prediction leverages the decorrelation among trees to enhance generalization performance. This strategy makes Extra Trees particularly effective for handling high-dimensional data, as well as datasets with noisy or redundant features. Compared to Random Forests, Extra Trees are computationally more efficient due to the elimination of the search for optimal split points, making them well-suited for large-scale regression tasks [51].

3.3.2. Gradient tree boosting regression

The Gradient Tree Boosting Regressor, also known as Gradient

Boosted Regression Trees (GBRT), is a powerful ensemble learning method that builds a strong predictive model by iteratively combining multiple weak learners, typically decision trees, in a stage-wise manner. Unlike Random Forests and Extra Trees, which average predictions from independently trained trees, gradient boosting builds trees sequentially, with each new tree trained to correct the residual errors of the previous trees. The method is grounded in gradient-based optimisation, where each new tree minimizes the residual loss using a differentiable loss function, leading to a refined and accurate predictive model.

Mathematically, given a dataset $\mathscr{D} = \{(x_i, y_i)\}_{i=1}^{N}$, where $x_i R^d$ represents the feature vector and $y_i \in R$ is the target variable, gradient boosting constructs an additive model of T decision trees. The model learns a function F(x) that approximates the mapping from input x to target y by iteratively refining its predictions as shown in Eq. 4:

$$F_T(x) = F_{T-1}(x) + \eta f_T(x) \tag{4}$$

where $f_T(x)$ is the prediction from the newly added decision tree at iteration T, andη(the learning rate) controls the contribution of each tree to the final model. The function $F_T(x)$ is initialized with a constant value, often the mean of the target variable as shown in Eq. 5:

$$F_0(x) = \underset{c}{\operatorname{argmin}} \sum_{i=1}^{N} L(y_i, c) \tag{5}$$

where $L(y,\widehat{y})$ is the chosen loss function, commonly the squared error for regression as shown in Eq. 6:

$$L(y, \widehat{y}) = (y - \widehat{y})^2 \tag{6}$$

At each iteration, a new tree is fitted to approximate the negative gradient of the loss function with respect to the current model's predictions as shown in Eq. 7:

$$r_i^{(t)} = -\left[\frac{\partial L(y_i, F_{t-1}(x_i))}{\partial F_{t-1}(x_i)}\right] \tag{7}$$

This residual $r_i^{(t)}$ serves as the pseudo-target for the next tree, which is then trained to minimize the mean squared error with respect to these gradients. The final prediction is obtained by summing the outputs of all trees in the ensemble as shown in Eq. 8:

$$\widehat{y}(x) = \sum_{t=1}^{T} \eta f_t(x) \tag{8}$$

One of the key advantages of Gradient Tree Boosting is its ability to model complex, non-linear relationships with high accuracy while maintaining strong generalization performance. The method can be regularized through techniques such as learning rate reduction, limiting tree depth, and incorporating shrinkage or subsampling to prevent overfitting. Compared to Random Forests and Extra Trees, gradient boosting often achieves superior predictive accuracy, particularly in structured data settings, though it requires careful hyperparameter tuning to balance bias-variance trade-offs [52,53].

3.3.3. Extreme gradient boosting (XGBoost)

The Extreme Gradient Boosting (XGBoost) Regressor is an optimized implementation of gradient tree boosting that enhances computational efficiency, scalability, and predictive accuracy. As a variant of Gradient Boosted Regression Trees (GBRT), XGBoost constructs an ensemble of decision trees in a stage-wise fashion, where each new tree corrects the residual errors of the previous trees. However, XGBoost introduces several key improvements over standard gradient boosting, including second-order gradient optimization, a regularized objective function, column block structure for parallelization, and sparsity-aware split finding, making it particularly well-suited for large-scale regression tasks.

Formally, given a dataset $\mathscr{D} = \{(x_i, y_i)\}_{i=1}^{N}$, where $x_i \in R^d$ represents the feature vector and $y_i \in R$ is the target variable, XGBoost builds an additive model of T trees to approximate the function F(x) that maps inputs to outputs as shown in Eq. 9:

$$F_T(x) = F_{T-1}(x) + \eta f_T(x) \tag{9}$$

Where $f_T(x)$ is the new decision tree added at iteration T, and η (the learning rate) controls its contribution. Unlike traditional gradient boosting, which optimizes using first-order gradients, XGBoost leverages a Taylor expansion of the loss function up to the second order to improve optimisation as shown in Eq. 10:

$$L(y, \widehat{y}) \approx L(y, F_{t-1}(x)) + g_i f_t(x) + \frac{1}{2} h_i f_t^2(x) \tag{10}$$

Where $g_i$and $h_i$are the first-order gradient and second-order Hessian of the loss function, respectively as shown in Eq. 11:

$$g_i = \frac{\partial L(y_i, F_{t-1}(x_i))}{\partial F_{t-1}(x_i)}, \quad h_i = \frac{\partial^2 L(y_i, F_{t-1}(x_i))}{\partial^2 F_{t-1}(x_i)} \tag{11}$$

By incorporating second-order derivatives, XGBoost achieves more precise updates, leading to faster convergence and improved predictive performance. Additionally, XGBoost regularizes the model using an objective function that includes both L1 (Lasso) and L2 (Ridge) penalties as shown in Eq. 12:

$$\Omega(f_t) = \gamma T + \frac{1}{2} \lambda \sum_{j=1}^{T} w_j^2 \tag{12}$$

where γ controls the complexity penalty for each tree, and λ regulates the magnitude of leaf weightsw_j. This regularization prevents overfitting and enhances generalization.

A major advantage of XGBoost is its efficient computation. By employing a column block structure for parallel tree construction and a sparsity-aware split-finding algorithm, XGBoost can handle high-dimensional data with missing values more efficiently than traditional boosting methods. The combination of gradient-based optimization, regularization, parallelization, and efficient memory usage makes XGBoost a state-of-the-art approach for regression tasks [54,55].

3.4. Shapley additive exPlanations (SHAP)

SHAP is a widely used method for interpreting ML model predictions by quantifying the contribution of each feature to the output. Based on cooperative game theory, SHAP assigns a Shapley value to each feature, ensuring a fair distribution of contributions by considering all possible feature combinations. This method provides a consistent and theoretically grounded approach to feature attribution, making it particularly valuable for understanding complex models. By illustrating both global and local feature importance, SHAP enhances model transparency and supports informed decision-making. In this study, SHAP analysis will be conducted on the best-performing model to assess the relative influence of each feature on its predictions [56].

3.5. Multi-objective optimization

Multi-objective optimization (MOO) is a critical approach in engineering and materials science, particularly for balancing competing objectives in structural design. In this study, Non-dominated Sorting Genetic Algorithm II (NSGA-II) was employed to simultaneously optimize the mechanical and ductility properties of composite RWS connections while incorporating an additional sustainability objective: minimizing total embodied carbon. The NSGA-II algorithm, a well-established evolutionary optimisation method, was chosen due to its efficiency in handling complex, multi-dimensional trade-offs and its ability to maintain a diverse set of Pareto-optimal solutions [57].

The optimization problem was formulated with eight objective functions, including the seven mechanical and ductility

properties—Yield Moment, Maximum Moment, Ultimate Moment, Equivalent Viscous Damping, Energy Dissipated, Ductility Under Hogging, and Ductility Under Sagging—alongside total embodied carbon reduction due to the opening in the web section. These objectives often exhibit conflicting behavior; for instance, enhancing strength and ductility may lead to increased material usage, thereby elevating embodied carbon emissions. Thus, an optimisation framework that simultaneously accounts for mechanical performance and sustainability is essential.

The embodied carbon (EC) calculations are based on the Institution of Structural Engineers (IStructE) guidelines [58]. The scope of the embodied carbon calculations was taking into account the life-cycle assessment for the modules A1–A5 as illustrated in Fig. 5, which focuses on the embodied carbon calculation up to practical completion stag referred to as cradle-practical completion. The embodied carbon factors (ECFs) for the structural steel sections were sourced from the British Steel Environmental Product Deceleration (EPD) [59]. Sustainability was quantified by calculating the total reduction in embodied carbon ($EC_{reduction}$) resulting from the web perforation. The weight removed was multiplied by the sum of the embodied carbon factors for modules A1–A3, A4, and A5w (2.45, 0.032, and 0.025, respectively) as shown in Eq. 13.

$$EC_{reduction} = W_{(removed)} \times (ECF_{(A1-A3)} + ECF_{A4} + ECF_{A5w}) \quad (13)$$

Where $W_{(removed)}$ represents the weight of the steel removed from the web section. The $EC_{reduction}$ value was integrated into the NSGA-II algorithm as a primary objective to be maximized. It is acknowledged that absolute carbon values may vary depending on assumptions such as material sourcing, manufacturing techniques, and installation practices; however, these variations do not alter the relative trends or the optimal trade-offs determined in this study.

To address constraints effectively, a custom repair operator was integrated into the NSGA-II algorithm to ensure feasible solutions by correcting infeasible candidates based on predefined structural constraints. Two primary constraints were applied: (1) all predictor variables were restricted to remain within the upper and lower bounds of the compiled dataset, ensuring that generated solutions represent realistic and physically attainable designs; and (2) the predicted yield moment was required to be less than or equal to the predicted maximum moment, maintaining mechanical consistency with established structural behavior. The optimisation process was carried out with a population size of 20 over 500 generations, leveraging constraint handling and duplicate elimination to enhance solution diversity and convergence toward an optimal trade-off front.

The NSGA-II algorithm operates by maintaining a Pareto front, where solutions are ranked based on dominance relationships, ensuring a diverse distribution of trade-off solutions between mechanical performance and sustainability [61,62]. By applying this evolutionary approach, the study identifies a set of optimal design alternatives that balance structural efficiency with environmental impact, aiding in the development of more sustainable and high-performance composite RWS connections.

3.6. User-friendly interface

A user-friendly interface was developed using Gradio V4.36.1 and deployed online via Hugging Face to facilitate predictive modeling in structural engineering. Following a comprehensive evaluation of multiple ensemble machine learning models, the best-performing model was selected based on its predictive accuracy and robustness. This optimized model enables precise estimation of seven mechanical properties—Yield Moment, Maximum Moment, Ultimate Moment, Equivalent Viscous Damping, Energy Dissipated, Ductility Under Hogging, and Ductility Under Sagging—along with total embodied carbon reduction. The Gradio interface allows researchers and engineers to seamlessly integrate this tool into their optimisation workflows, supporting data-driven decision-making. The trained model files and source code are available at the following link: (https://huggingface.co/spaces/MohamedRabie26/RWS_connections/tree/main).

4. Criteria for performance evaluation & hyperparameter selection

4.1. Performance evaluation criteria

Optimal outcomes in data-driven models require continuous performance assessment during training. In this study, the Optuna library was used for efficient hyperparameter optimisation. Each machine

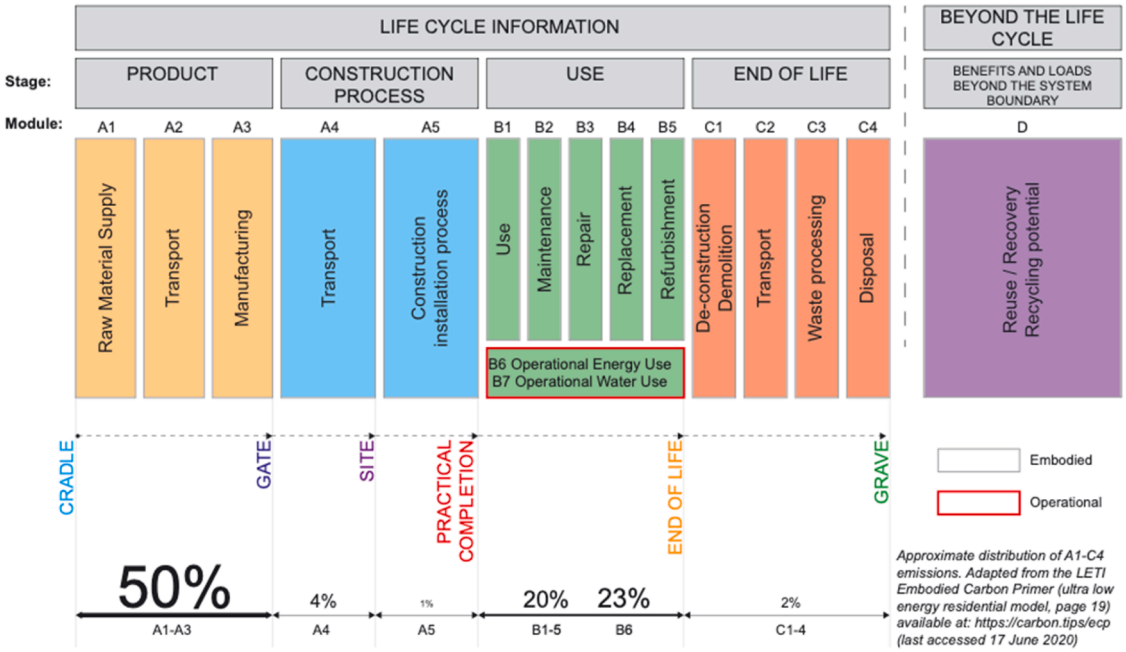

Fig. 5. Life cycle assessment stages and modules [60].

learning model was trained and tuned using 10-fold cross-validation, in which the training dataset was randomly partitioned into ten equal subsets. In each fold, nine subsets were used for training and one for validation, cycling through all combinations. The final model configuration was chosen based on the average validation performance across the folds, ensuring robust hyperparameter selection and improved generalization to unseen data. This approach was preferred over holding out an additional independent dataset, as it allows for efficient use of the available data while still providing multiple rigorous evaluations on unseen subsets, thereby reducing the risk of overfitting. The performance of different ML models was evaluated using four metrics: Mean Absolute Percentage Error (MAPE), Mean Absolute Error (MAE), Root Mean Squared Error (RMSE), and the Coefficient of Determination (R^2), as defined in Eqs. 14–17:

$$MAPE = \frac{100}{n}\sum_{i=1}^{n}\left|\frac{y_i - \hat{y}_i}{y_i}\right| \tag{14}$$

$$MAE = \frac{1}{n}\sum_{i=1}^{n}|y_i - \hat{y}_i| \tag{15}$$

$$RMSE = \sqrt{\frac{1}{n}\sum_{i=1}^{n}(y_i - \hat{y}_i)^2} \tag{16}$$

$$R^2 = 1 - \frac{\sum_{i=1}^{n}(y_i - \hat{y}_i)^2}{\sum_{i=1}^{n}(y_i - \bar{y})^2} \tag{17}$$

where $y_i$and $\hat{y}_i$ are the target and predicted values, respectively, $\bar{y}$ is the mean of values, and n is the number of data points.

A brief description of the statistical metrices used in evaluating each ML model is as follows:

- Mean Absolute Percentage Error (MAPE): MAPE measures the average percentage deviation between predicted and actual values, providing an intuitive understanding of prediction accuracy. It is particularly useful for comparing model performance across different datasets with varying scales.
- Mean Absolute Error (MAE): MAE quantifies the average magnitude of errors in predictions, without considering their direction. Its straightforward interpretation makes it a reliable metric for assessing the overall prediction quality of machine learning models.
- Root Mean Squared Error (RMSE): RMSE highlights the magnitude of larger errors by giving more weight to significant deviations due to its squaring process. This makes it an essential metric for detecting models that fail to capture extreme variations in the mechanical properties of AAM.
- Coefficient of Determination (R^2): R^2 measures the proportion of variance in the target variable explained by the model. It is critical for understanding how well a model captures the underlying patterns in the data, reflecting its overall goodness-of-fit.

These metrics collectively provide a comprehensive evaluation framework, ensuring that both accuracy and robustness of the machine learning models are effectively assessed for predicting the mechanical and ductility properties of RWS connections.

A superior model exhibits lower MAE and RMSE values, coupled with a higher R^2 value. Where overfitting of a model shows higher error metrics on the test set compared to the training set and a significant discrepancy between training and test R^2values.

4.2. Hyper parameter selection

Hyperparameters are critical for the performance and accuracy of a ML model, requiring careful optimisation. This study uses Optuna, a robust hyperparameter optimization framework, to fine-tune model parameters. Optuna is more efficient and flexible than traditional grid search, effectively handling high-dimensional and non-convex parameter spaces. It also prunes unpromising trials early, saving computational resources. Detailed optimized hyperparameter values and best-performing settings are summarized in Table 3. Further information on Optuna can be found in [63].

5. Results and discussion

5.1. Performance evaluation and explainability analysis of ML models for RWS connections

Table 4 presents the performance indices for three machine learning models—Extra Trees Regressor (ETR), Gradient Tree Boosting Regressor (GTBR), and Extreme Gradient Boosting (XGBoost)—in predicting seven key outputs for Reduced Web Section (RWS) connections. The models were evaluated based on Mean Absolute Percentage Error (MAPE %), Mean Absolute Error (MAE), Root Mean Square Error (RMSE), and the coefficient of determination (R^2) for both the training and test datasets. A comparative analysis of these metrics provides insights into the predictive accuracy and generalization ability of each model across different mechanical properties.

5.1.1. Yield moment

The performance evaluation of ML models for predicting Yield Moment (M_y) demonstrates that XGBoost is the most effective model, achieving the lowest test MAPE (5.206 %) and the highest R^2 (0.99), indicating superior generalization capability. While ETR exhibited the lowest training error (MAPE: 2.312 %), its higher test error (MAPE: 7.034 %) suggests mild overfitting, whereas GTBR maintained a balanced performance with an R^2 of 0.982 on the test dataset. To further understand the contribution of input features to model predictions, SHAP analysis was performed on the optimal ML model as shown in Fig. 6, revealing that the cross-sectional area of the beam (A_a) is the most influential feature, followed by web thickness (t_{bw}), flange thickness (t_{bf}), column depth (h_c), and column flange thickness (t_{cf}). These results align with fundamental structural mechanics principles [64], where larger cross-sectional dimensions in particular the distance between the flanges, the higher the distance the higher the moment capacity. The connection type also plays a notable role, with the “welded” connection type showing a substantial impact on Yield Moment prediction, highlighting the significance of stress transfer mechanisms at the connection interface [65]. Features such as column length (L_c), radius of gyration (r_y), and column yield strength ($f_{yn}(column)$) were found to have minimal influence, suggesting that their contribution to M_y is relatively indirect. The SHAP summary plot further indicates non-linear feature interactions, particularly for A_a, which exhibits a stronger influence at higher values. These insights reinforce the model’s reliability and interpretability, demonstrating that the machine learning framework successfully captures the underlying structural behavior of RWS connections.

5.1.2. Maximum moment

The performance evaluation of ML models in predicting Maximum Moment (M_m) indicates that XGBoost is the most reliable model, achieving the highest R^2 value (0.994) and the lowest test RMSE (0.012), signifying strong predictive accuracy and generalization. While ETR exhibited the lowest training error (MAPE: 4.183 %), its test error (MAPE: 7.835 %) suggests a degree of overfitting, whereas GTBR performed competitively with a test R^2 of 0.989, showing balanced performance. To gain further insight into the contribution of individual features to the model’s predictions, SHAP analysis was conducted on the optimal ML model as shown in Fig. 7. The results demonstrate that flange thickness (t_{bf}) is the most significant predictor, followed closely by cross-sectional area (A_a), web thickness (t_{bw}), and beam height (h_b), all of which play a crucial role in governing the flexural capacity of RWS

Table 3
Optuna optimized hyperparameters.

Model	Hyperparameter Range	M_y	M_m	M_u	Ed	ζeq	θ_u/θ_y +ve	θ_u/θ_y -ve
Extra tree regressor (ETR)	max_depth: [3, 500]	375	311	299	268	141	12	89
-	max_features: ['log2', 'sqrt']	sqrt	log2	sqrt	sqrt	log2	log2	sqrt
-	min_samples_leaf: [1, 50]	1	1	1	1	9	1	1
-	min_samples_split: [2, 100]	2	4	5	10	1	2	6
-	n_estimators: [10, 1000]	228	928	917	78	283	558	111
-	random_state: [5]	5	5	5	5	5	5	5
Gradient tree boosting (GTB)	n_estimators: [50, 2000]	1527	1846	620	86	232	1919	178
-	max_depth: [4, 100]	78	4	4	9	96	45	74
-	learning_rate: [0.01, 0.9]	0.074	0.165	0.318	0.168	0.095	0.010	0.089
-	subsample: [0.2, 0.9]	0.455	0.615	0.370	0.802	0.719	0.888	0.807
-	max_features: [7, 100]	7	7	7	7	9	95	10
-	min_samples_split: [2, 50]	25	14	47	24	46	48	47
-	min_samples_leaf: [1, 50]	19	23	14	28	27	7	6
-	random_state: [5]	5	5	5	5	5	5	5
Extreme gradient boosting (XGBoosting)	n_estimators': [50, 2000],	1464	1775	1062	1557	851	1467	1132
-	'max_depth': [4, 40],	35	5	23	29	30	28	8
-	'learning_rate': [0.01, 0.99],	0.071	0.065	0.500	0.210	0.233	0.101	0.104
-	'subsample': [0.1, 0.9],	0.587	0.802	0.704	0.869	0.776	0.547	0.736
-	'colsample_bylevel': [0.1, 0.9],	0.880	0.421	0.750	0.795	0.848	0.562	0.304
-	'colsample_bynode': [0.1, 1.0],	0.458	0.570	0.511	0.401	0.911	1.000	0.976
-	'colsample_bytree': [0.1, 1.0],	0.818	0.835	0.628	0.983	0.414	0.740	0.858
-	'reg_alpha': [0, 0.9],	2.03E-05	0.016	0.158	0.886	0.198	0.426	0.066
-	'reg_lambda': [0.1, 1],	0.849	0.902	0.892	0.867	0.739	0.566	0.813
-	'gamma': [0.0, 0.1],	1.20E-04	1.39E-05	7.94E-05	0.00118749	6.42E-05	3.37E-05	0.0018
-	'random_state': [5]	5	5	5	5	5	5	5

Table 4
Performance indices for different ML algorithms in predicting outputs for RWS connections.

		Training dataset				Test dataset			
Output	Models	MAPE (%)	MAE	RMSE	R^2	MAPE (%)	MAE	RMSE	R^2
M_y	ETR	2.312	0.002	0.00320	0.999	7.034	0.008	0.017	0.984
	GTBR	2.968	0.003	0.00504	0.998	6.169	0.007	0.018	0.982
	XGBoosting	3.906	0.004	0.00542	0.998	5.206	0.006	0.013	0.99
M_m	ETR	4.183	0.005	0.00752	0.997	7.835	0.009	0.016	0.989
	GTBR	4.579	0.005	0.00818	0.997	6.746	0.008	0.015	0.989
	XGBoosting	4.572	0.005	0.00725	0.998	6.856	0.007	0.012	0.994
M_u	ETR	5.641	0.007	0.01062	0.996	8.916	0.010	0.017	0.987
	GTBR	6.727	0.008	0.01089	0.995	7.936	0.009	0.017	0.987
	XGBoosting	7.347	0.008	0.01146	0.994	8.117	0.009	0.014	0.991
Ed	ETR	7.626	0.015	0.03650	0.909	11.577	0.022	0.059	0.808
	GTBR	8.388	0.016	0.03421	0.917	14.535	0.024	0.075	0.698
	XGBoosting	8.322	0.016	0.03200	0.929	13.411	0.024	0.076	0.685
ζeq	ETR	2.981	0.013	0.02028	0.956	4.343	0.018	0.028	0.904
	GTBR	3.509	0.014	0.02392	0.937	4.717	0.018	0.03	0.891
	XGBoosting	2.856	0.013	0.01916	0.961	4.216	0.018	0.028	0.908
θ_u/θ_y +ve	ETR	2.55	0.014	0.02185	0.975	5.76	0.033	0.063	0.756
	GTBR	1.982	0.011	0.02033	0.978	6.574	0.038	0.068	0.714
	XGBoosting	3.785	0.019	0.02746	0.959	5.099	0.029	0.051	0.842
θ_u/θ_y -ve	ETR	4.051	0.025	0.03445	0.954	6.386	0.041	0.065	0.801
	GTBR	3.579	0.022	0.03150	0.962	6.145	0.040	0.064	0.808
	XGBoosting	4.122	0.026	0.03488	0.954	5.711	0.036	0.059	0.839

connections. The radius of gyration (r_y) and column flange thickness (t_{cf}) also exhibit substantial influence, reinforcing the importance of section stiffness and moment resistance. Interestingly, connection type (e.g., "Pre-Northridge") is moderately impactful, suggesting that different connection configurations influence moment transfer efficiency. Features such as beam flange width (b_f), column yield strength (fyn(column)), and column length (L_c) have minimal impact, indicating that local cross-sectional properties have a stronger influence than global structural dimensions. The SHAP summary plot further highlights that higher values of t_{bf} and A_a are positively correlated with increased M_m, aligning with fundamental structural mechanics principles where larger cross-sectional dimensions enhance moment capacity [66]. These findings confirm that the XGBoost model effectively captures the non-linear dependencies governing Maximum Moment, and the SHAP analysis reinforces the physical consistency of the model's predictions.

5.1.3. Ultimate moment

The evaluation of ML models for predicting Ultimate Moment (M_u) reveals that XGBoost provides the most reliable generalization, achieving an R^2 of 0.991 on the test dataset, coupled with the lowest test RMSE (0.014). While ETR performed well on the training dataset with the lowest MAPE (5.641 %), its test performance (MAPE: 8.916 %) suggests a tendency toward overfitting, whereas GTBR maintained a balanced performance (test MAPE: 7.936 %). To further interpret the model's decision-making process, SHAP analysis was conducted to quantify the influence of each feature on Ultimate Moment predictions using the optimum ML model as shown in Fig. 8. The results indicate that cross-sectional area (A_a) and beam height (h_b) are the most dominant predictors, highlighting their fundamental role in resisting flexural forces. Flange thickness (t_{bf}), column flange thickness (t_{cf}), and column depth (h_c) also exhibit a strong influence, emphasizing the importance of both beam and column stiffness in moment capacity. Interestingly, the

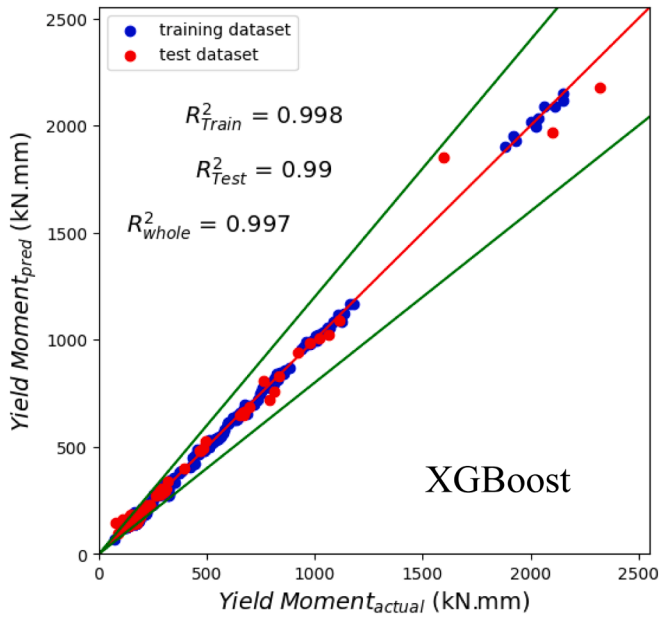

(a)

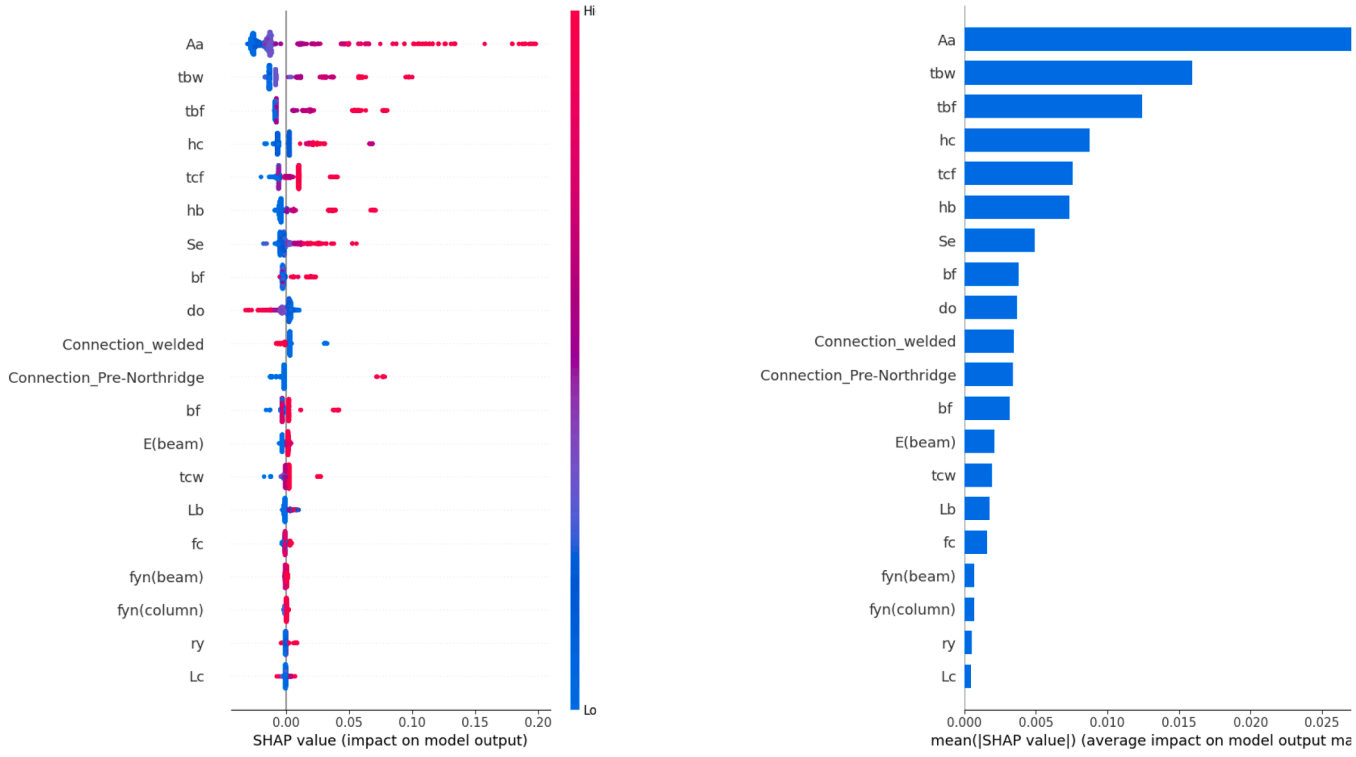

(b) (c)

Fig. 6. Performance of the optimum ML model in predicting the yield moment of RWS connection; (a) Comparison of actual vs. predicted values; (b) SHAP summary plot of the predictions; (c) Ranking of feature's impact on the prediction model.

diameter of the openings (do) appears to have a significant impact, likely due to its effect on stress redistribution within the reduced web section. The SHAP summary plot suggests that increasing A_a,h_b, and tbf generally leads to higher M_u, which is consistent with structural mechanics principles. The influence of connection type (e.g., "welded") is moderate, indicating that while connection properties affect moment transfer, the primary governing factors are section dimensions. Features such as beam yield strength (fyn_{beam}), column elastic modulus (E_{col}), and column length (L_c) have minimal impact, reaffirming that local cross-sectional properties and geometry are the primary drivers of Ultimate Moment capacity [67].

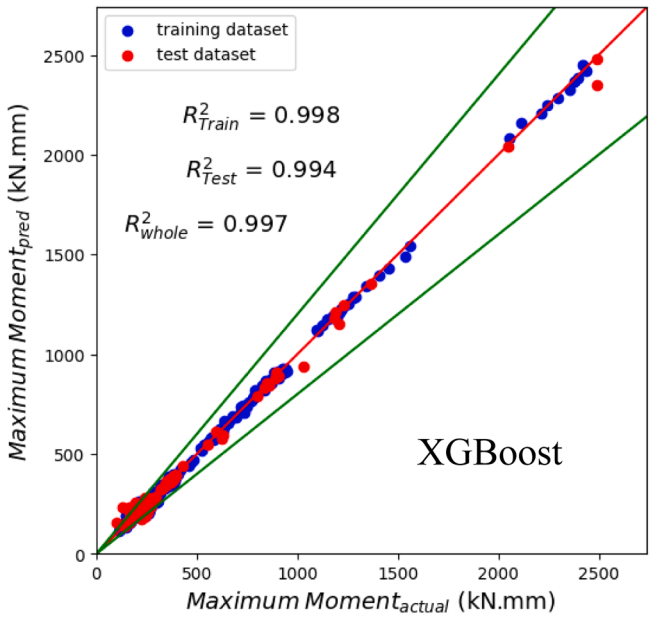

(a)

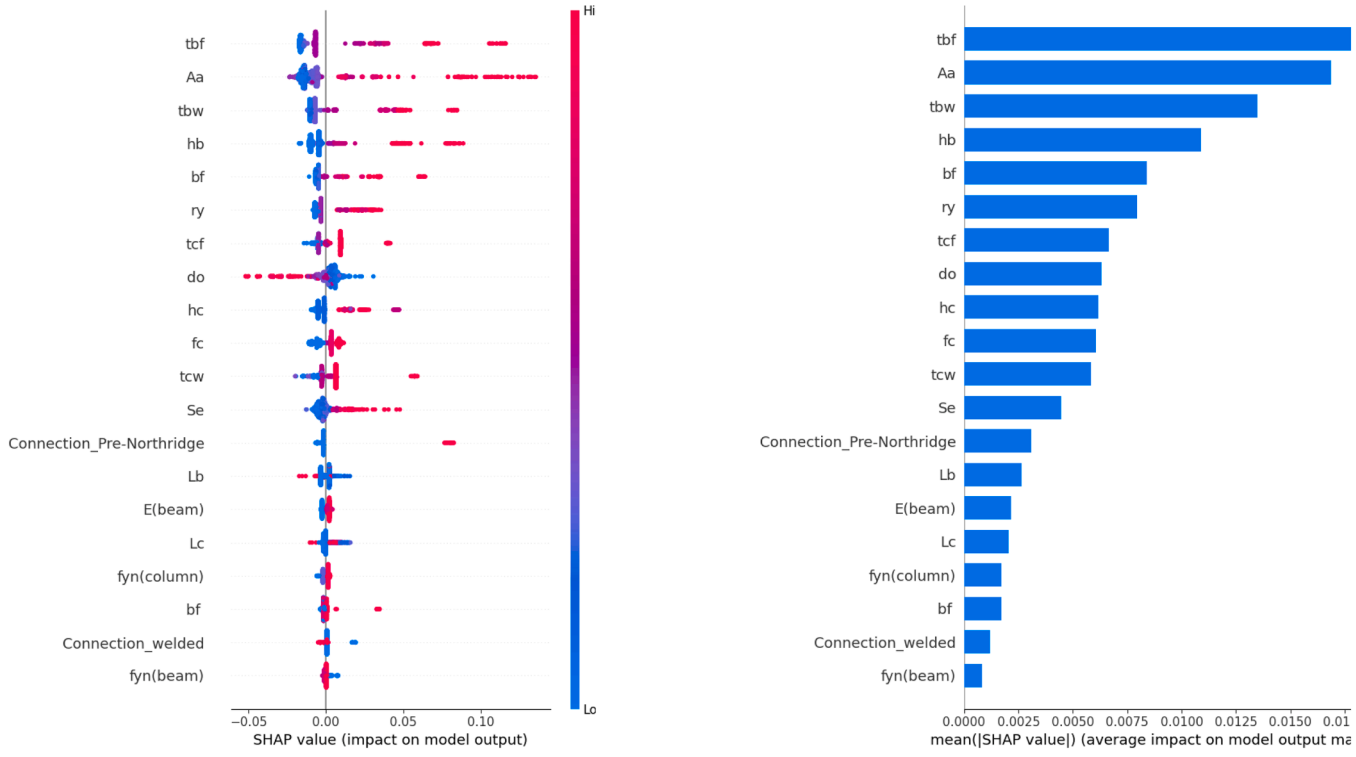

(b) (c)

Fig. 7. Performance of the optimum ML model in predicting the maximum moment of RWS connection; (a) Comparison of actual vs. predicted values; (b) SHAP summary plot of the predictions; (c) Ranking of feature's impact on the prediction model.

5.1.4. Dissipated energy

The evaluation of machine learning models for predicting Dissipated Energy (E_d) reveals that while all three models exhibit reasonable accuracy, XGBoost outperforms the others in generalization, achieving an R^2 of 0.929 on the training dataset, though its test R^2 drops to 0.685, indicating potential overfitting or the inherent complexity of predicting energy dissipation. ETR performed slightly better in terms of test generalization (R^2 = 0.808), while GTBR showed the lowest performance on the test set (R^2 = 0.698). While XGBoost demonstrated superior predictive accuracy for most outputs, the Extra Trees Regressor provided a higher R^2 value for energy dissipated (E_d)) on the testing dataset (0.808 vs. 0.685). This metric is particularly sensitive to local

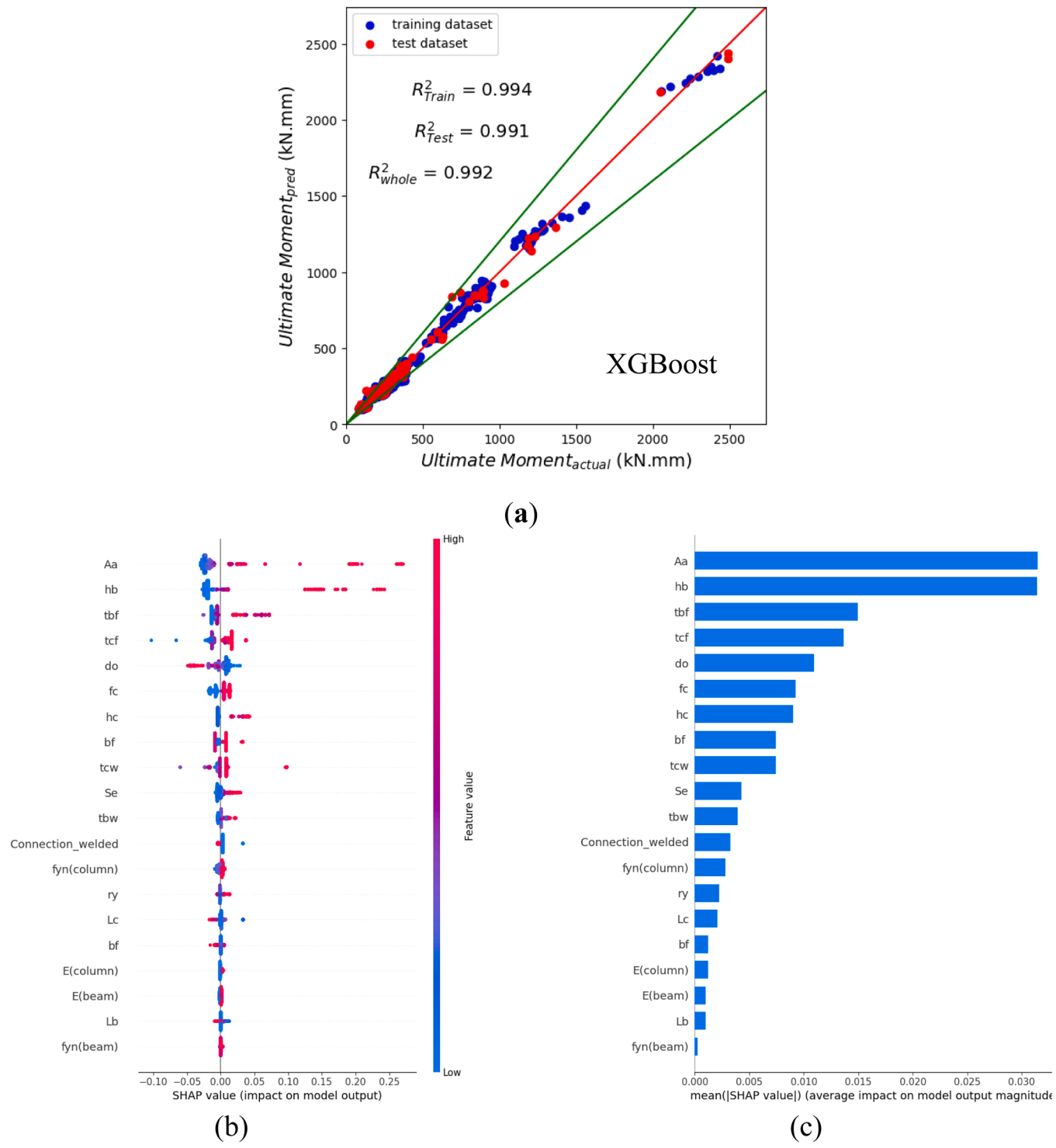

Fig. 8. Performance of the optimum ML model in predicting the ultimate moment of RWS connection; (a) Comparison of actual vs. predicted values; (b) SHAP summary plot of the predictions; (c) Ranking of feature's impact on the prediction model.

connection details and cyclic loading history, making its prediction more challenging. For subsequent optimization, the best-performing model for each output in the testing dataset was selected to ensure robust and objective-driven predictions. To further investigate the factors influencing dissipated energy predictions, SHAP analysis was performed on the optimum ML model as illustrated in Fig. 9. The results highlight that beam elastic modulus (E_{beam}) is the most dominant predictor, followed by flange thickness (t_{bf}), cross-sectional area (A_a), column height (h_c), and column flange thickness (t_{cf}). This indicates that energy dissipation is strongly influenced by the stiffness properties of the beam and column, as well as the overall section geometry, which govern plastic deformation capacity and hysteretic behavior.

The SHAP summary plot further reveals that higher values of E_{beam} and t_{bf} correspond to increased dissipated energy, which aligns with structural mechanics principles, as stiffer beams and thicker flanges enhance plastic energy dissipation. Additionally, web thickness (t_{bw}) and yield strength of the beam (fyn_{beam}) show moderate influence, suggesting that material strength also plays a crucial role. Interestingly,

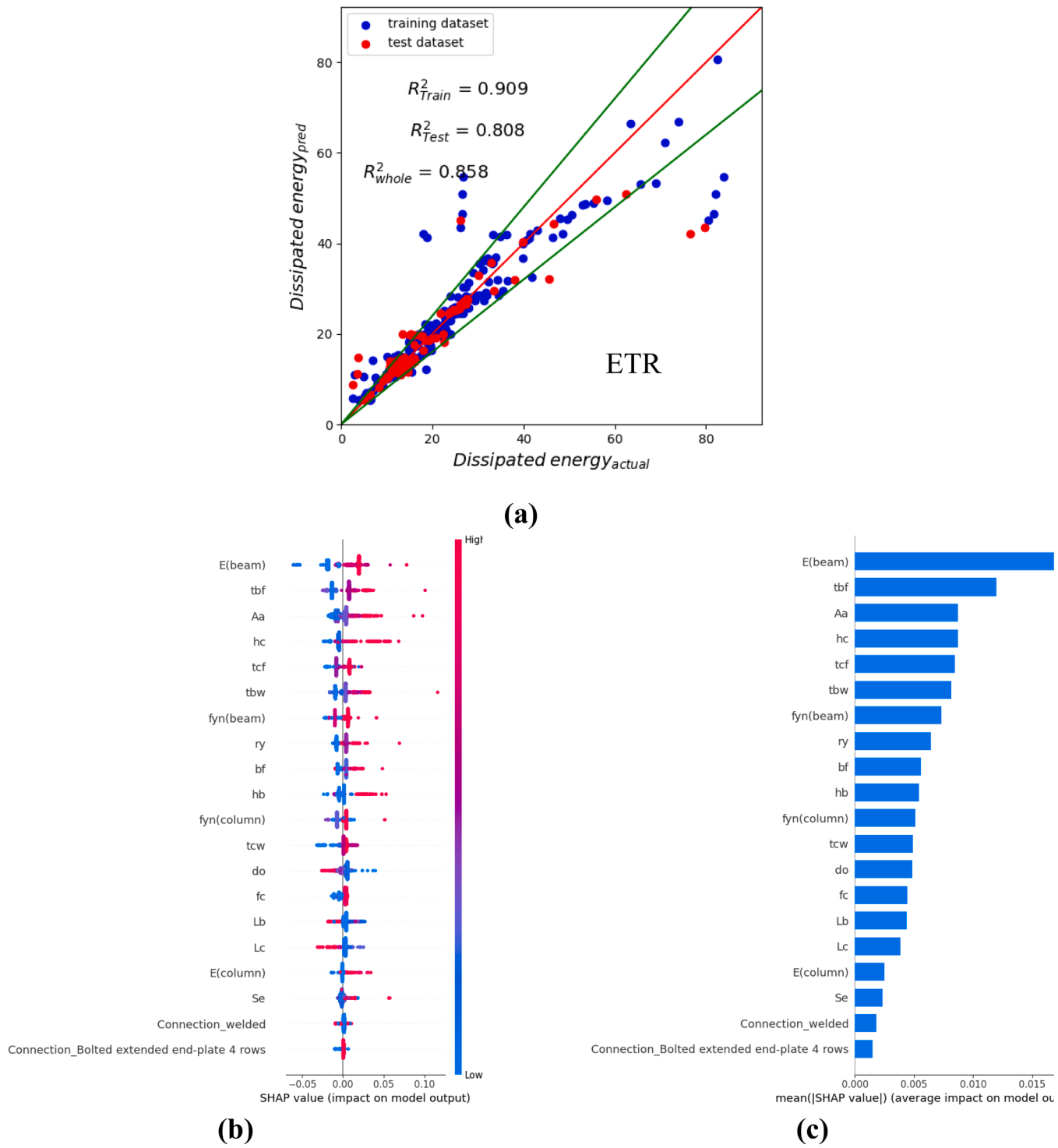

Fig. 9. Performance of the optimum ML model in predicting the dissipated energy of RWS connection; (a) Comparison of actual vs. predicted values; (b) SHAP summary plot of the predictions; (c) Ranking of feature's impact on the prediction model.

connection type (e.g., "Bolted extended end-plate 4 rows") has a minor influence, indicating that while connections contribute to energy dissipation, the primary governing factors are the material and geometric properties of the beam and column rather than the connection detailing. Lower-ranked features such as column elastic modulus (E_{col}) and column yield strength (fyn_{column}) exhibit minimal impact, reinforcing the notion that beam behavior is more critical than column properties in determining dissipated energy [68,69].

These findings highlight the complexity of modelling energy dissipation, as it is governed by non-linear interactions between material properties, section geometry, and plastic hinge formation. While XGBoost provides the most robust predictions, the SHAP analysis suggests that further refinement, possibly incorporating additional hysteresis-related parameters, could enhance the model's predictive power.

5.1.5. *Equivalent viscous damping*

The ML models used to predict Equivalent Viscous Damping (ζeq)

demonstrated high predictive accuracy, with XGBoost achieving the lowest test MAPE (4.216 %) and the highest R^2(0.908), indicating superior generalization. While ETR achieved the lowest training error (MAPE: 2.981 %), its test error (MAPE: 4.343 %) was slightly higher, suggesting some degree of overfitting, whereas GTBR maintained balanced performance with an R^2 of 0.891, confirming its ability to capture the damping characteristics effectively. To better understand the influence of different features on ζeq, SHAP analysis was conducted to interpret the optimum model's predictions as shown in Fig. 10. The results indicate that flange thickness (t_{bf}) and cross-sectional area (A_a) are the most dominant predictors, highlighting their role in influencing damping behavior by affecting energy dissipation and stiffness. The diameter of the opening (do) and column length (L_c) also have a significant impact, suggesting that the presence of web openings and overall beam-column geometry contribute to damping capacity. The elastic modulus of the beam (E_{beam}) and beam length (L_b) further influence damping, reinforcing the notion that stiffness properties and beam flexibility contribute to energy dissipation mechanisms.

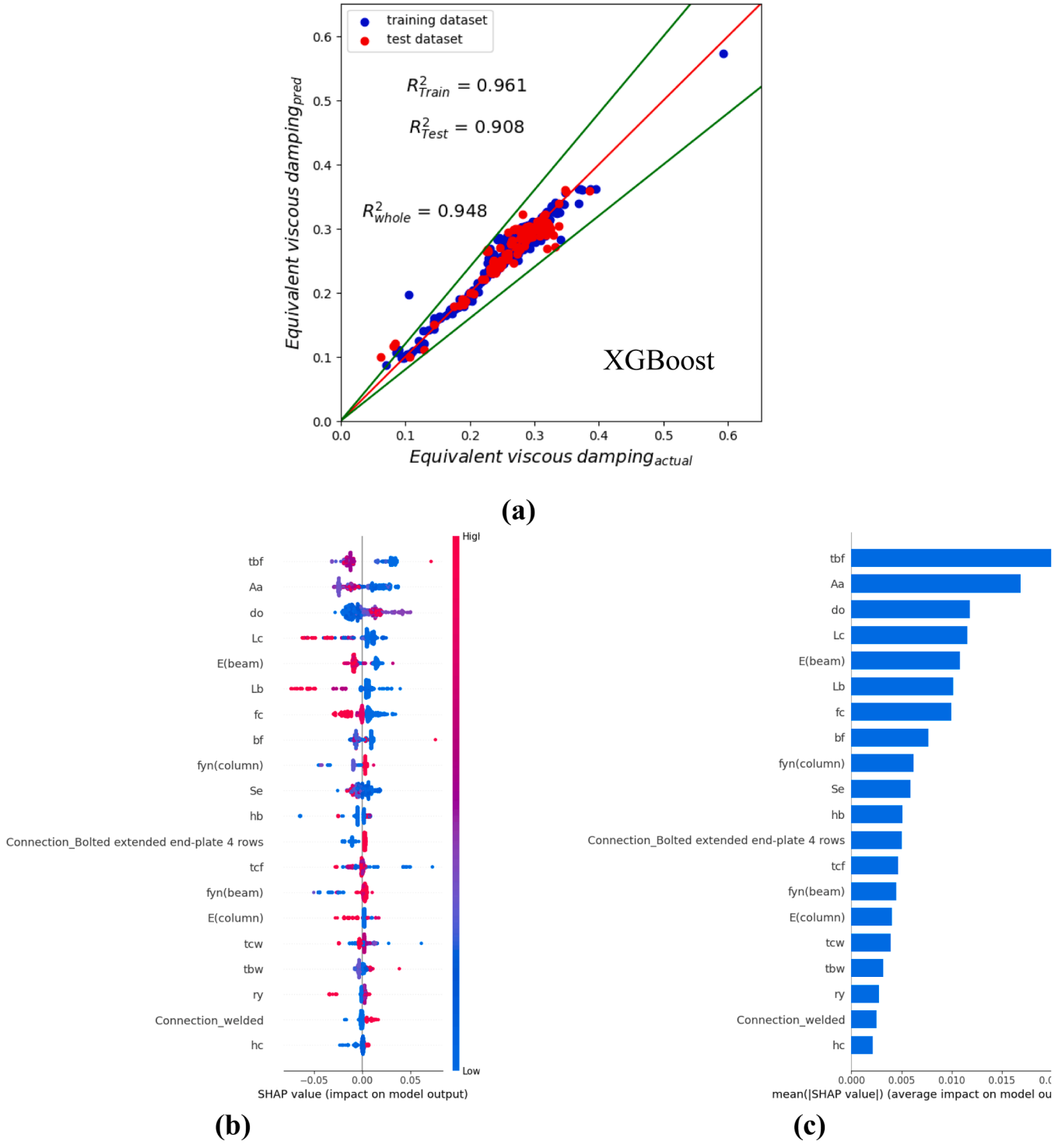

Fig. 10. Performance of the optimum ML model in predicting the equivalent viscous damping of RWS connection; (a) Comparison of actual vs. predicted values; (b) SHAP summary plot of the predictions; (c) Ranking of feature's impact on the prediction model.

The SHAP summary plot further reveals that higher values of t_{bf},A_a, and *do* generally lead to increased ζeq, which is consistent with structural behavior where larger cross-sections and web openings influence damping capacity by modifying deformation characteristics. Additionally, the connection type ("Bolted extended end-plate 4 rows") shows moderate influence, indicating that while connection configuration affects damping, material and geometric factors are the primary determinants. Features such as column flange thickness (t_{cf}), beam yield strength (fyn_{beam}), and column elastic modulus (E_{col}) have a lower impact, suggesting that the energy dissipation mechanism is predominantly governed by local section properties rather than global material strength. Interestingly, welded connections and column height (h_c) exhibit minimal influence, implying that while these factors contribute to overall structural behavior, they play a less significant role in damping capacity [70,71].

These findings reinforce the physical consistency of the ML model, demonstrating that XGBoost effectively captures the relationship between stiffness, energy dissipation, and damping behavior. The SHAP

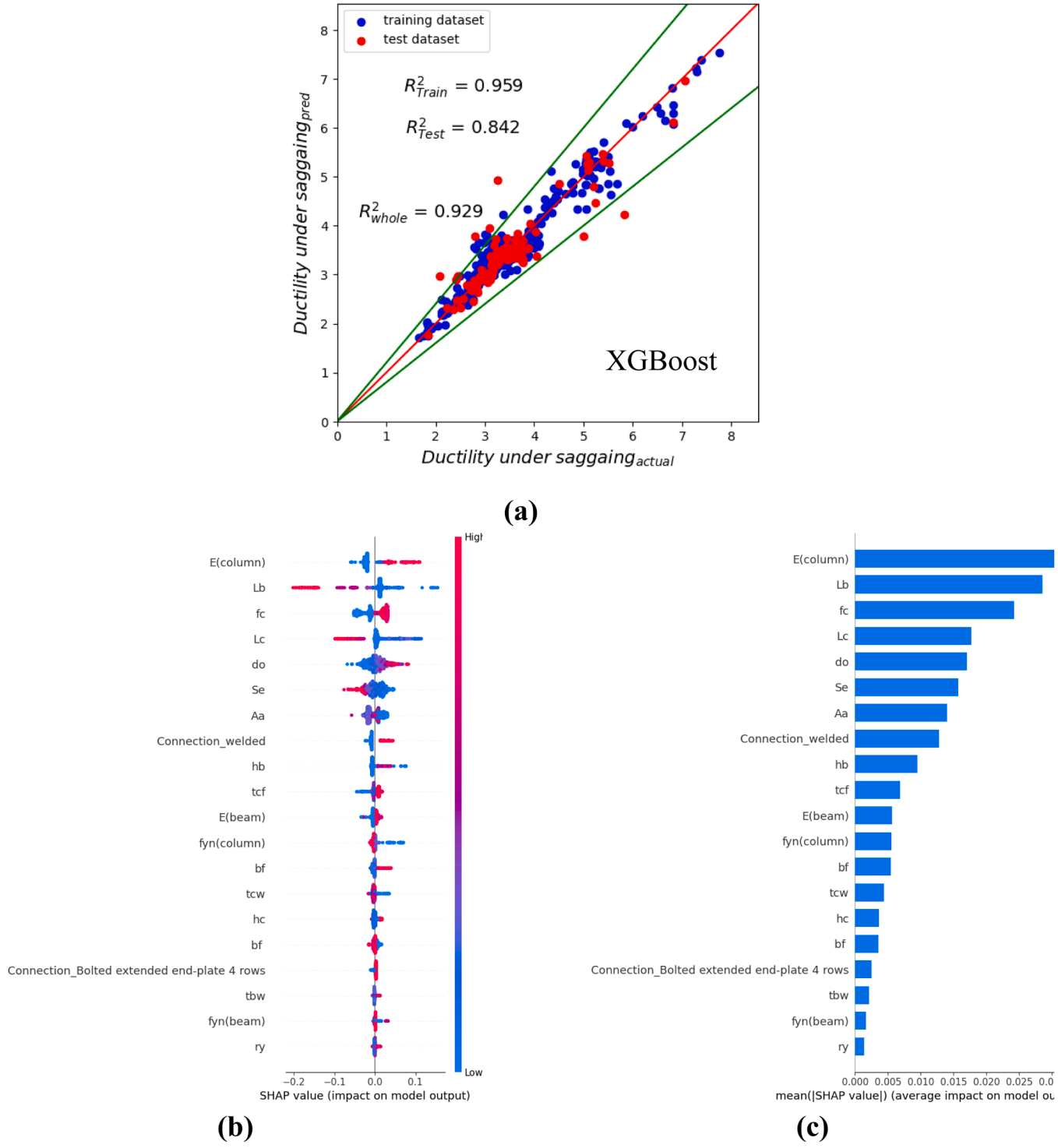

Fig. 11. Performance of the optimum ML model in predicting the ductility under sagging of RWS connection; (a) Comparison of actual vs. predicted values; (b) SHAP summary plot of the predictions; (c) Ranking of feature's impact on the prediction model.

analysis validates the importance of beam and web geometry, stiffness properties, and connection details in determining ζeq.

5.1.6. Ductility under sagging

The prediction of Ductility Under Sagging (θ_u/θ_y +ve) using ML models demonstrates that XGBoost achieves the best generalization performance, with the lowest test MAPE (5.099 %) and the highest R^2 (0.842), indicating its strong capability to capture the nonlinear relationships governing ductility behavior. ETR exhibited the lowest training error (MAPE: 2.55 %), but its test MAPE (5.76 %) suggests slight overfitting. Meanwhile, GTBR showed a higher test MAPE (6.574 %), which indicates a moderate generalization capability but a slight tendency to underperform in unseen data. The SHAP analysis was conducted to further interpret the feature contributions to model predictions as shown in Fig. 11. The results reveal that column elastic modulus (E_{column}) is the most influential predictor, followed by beam length (L_b), concrete compressive strength (f_c), column length (L_c), and the diameter of the web opening (d_o). These features significantly impact

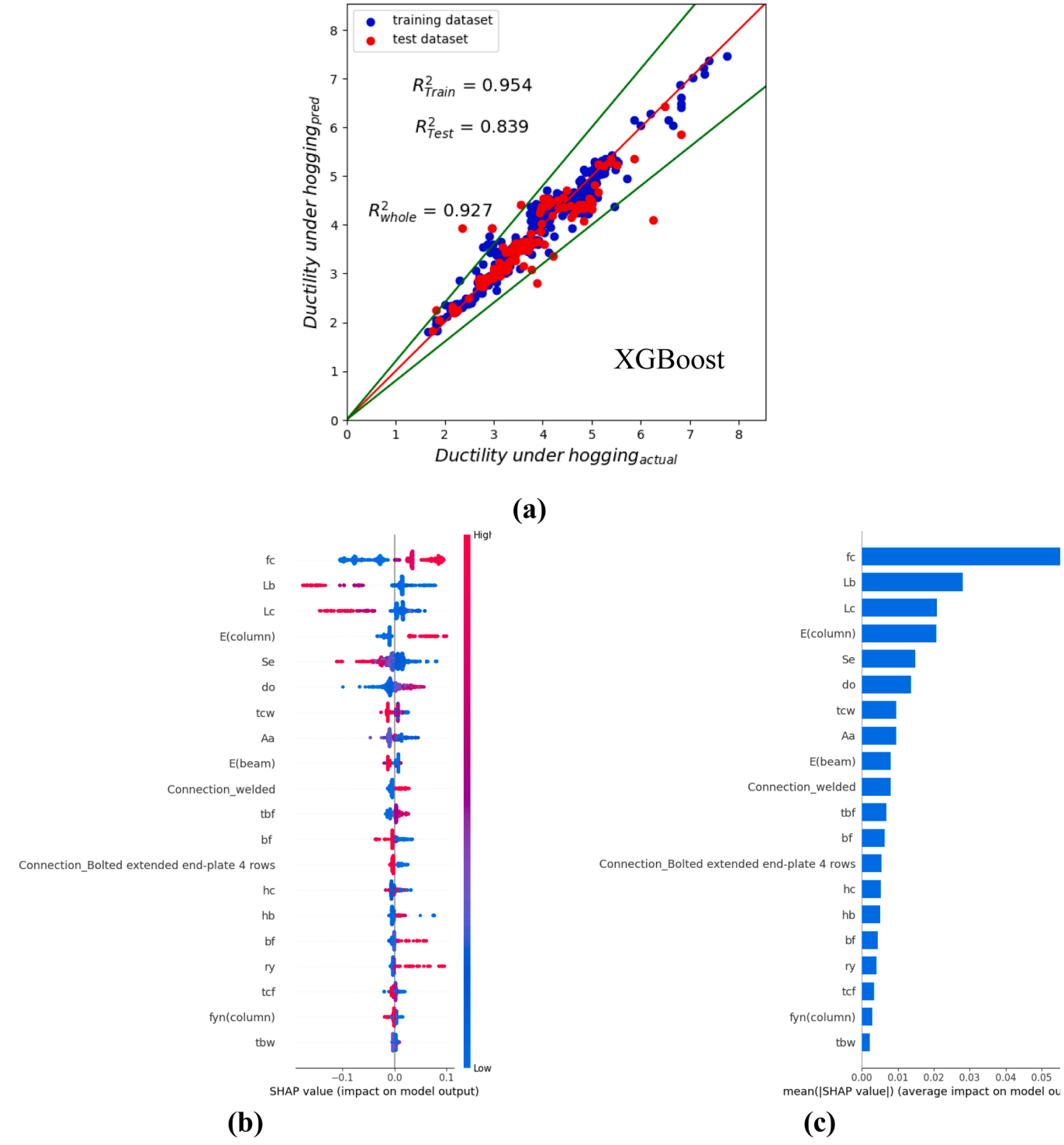

Fig. 12. Performance of the optimum ML model in predicting the ductility under hogging of RWS connection; (a) Comparison of actual vs. predicted values; (b) SHAP summary plot of the predictions; (c) Ranking of feature's impact on the prediction model.

ductility by influencing deformation capacity, material stiffness, and load redistribution mechanisms.

The SHAP summary plot indicates that higher values of E_{column} and L_b are associated with increased ductility, aligning with structural mechanics principles where greater column stiffness and longer beams enhance deformation capacity under sagging moments. The presence of web openings (d_o) plays a notable role, as it affects local buckling and energy dissipation mechanisms. The size and location of web opening (d_o and S_e) also exhibit moderate importance, reinforcing their role in determining the plastic rotation capacity. Interestingly, connection type (e.g., "welded" or "Bolted extended end-plate 4 rows") has a measurable impact, though it is not as dominant as material and geometric factors, suggesting that while connection stiffness influences ductility, the overall structural configuration and material behavior are the primary drivers. Features such as beam flange thickness (t_{bf}), web thickness (t_{bw}), and beam yield strength (fyn_{beam}) show a lower contribution, indicating that local cross-sectional parameters contribute less significantly to ductility compared to global stiffness and geometry effects [65,72].

These findings suggest that ductility under sagging moments is primarily controlled by column stiffness, beam length, and web opening effects, while connection type and beam cross-section play a secondary role.

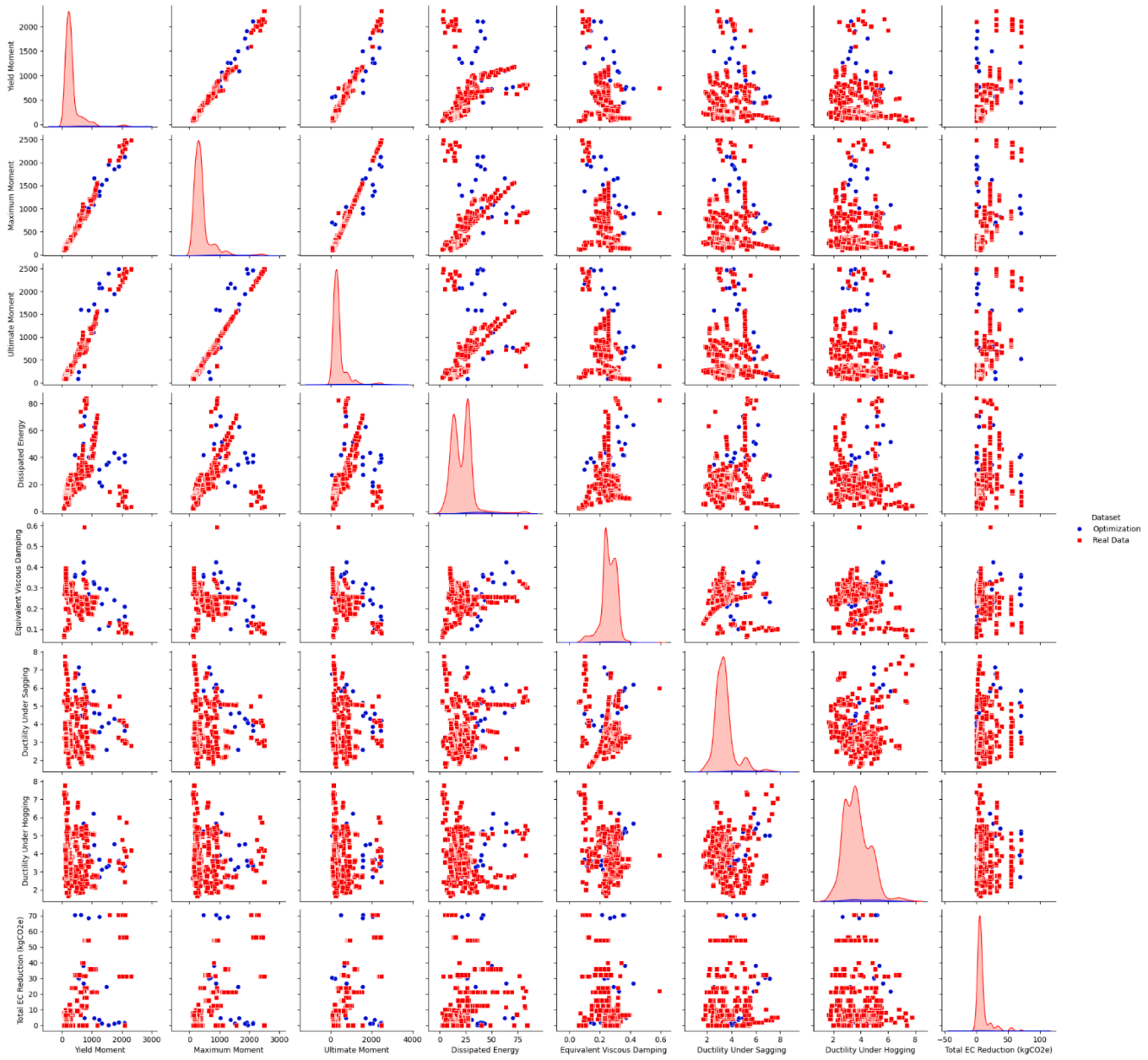

Fig. 13. Multi-objective optimisation for RWS connections with 7 output variables and total embodied carbon reduction.

5.1.7. Ductility under hogging

The prediction of Ductility Under Hogging (θ_u/θ_y -ve) using machine learning models shows that XGBoost provides the most accurate generalization, achieving the highest test R^2 (0.839) and the lowest test MAPE (5.711 %), suggesting its effectiveness in capturing the complex relationships governing ductility behavior under hogging moments. ETR exhibited the lowest training error (MAPE: 4.051 %), but its test error (MAPE: 6.386 %) was slightly higher, indicating some overfitting, whereas GTBR maintained relatively balanced performance (test MAPE: 6.145 %). To gain further insight into the model's decision-making process, SHAP analysis was performed to quantify feature importance and their impact on predictions as shown in Fig. 12. The results indicate that concrete compressive strength (f_c) is the most influential predictor, followed by beam length (L_b), column length (L_c), column elastic modulus (E_{column}), and section modulus (Se). These features significantly affect ductility by governing the stiffness, load redistribution, and deformation capacity of the system.

The SHAP summary plot suggests that higher values of f_c,L_b, and E_{column} are positively correlated with increased ductility, which is consistent with structural mechanics principles, where greater stiffness, increased member length, and improved concrete strength contribute to enhanced deformation capacity under hogging moments. Additionally, the diameter of web openings (d_o) and total cross-sectional area (A_a) exhibit moderate influence, indicating that web openings and section geometry affect the plastic hinge formation and rotational capacity of the connection. Interestingly, connection type (e.g., "welded" or "Bolted extended end-plate 4 rows") has a measurable impact, suggesting that while connection detailing contributes to ductility, the primary governing factors are material properties and global geometry. Lower-ranked features such as flange thickness (t_{bf}), web thickness (t_{bw}), and column yield strength (fyn_{column}) exhibit minimal influence, reinforcing that ductility is predominantly influenced by stiffness and member length rather than local cross-sectional properties [73].

These findings emphasize that ductility under hogging moments is primarily controlled by material strength (especially concrete compressive strength), beam and column stiffness, and geometric properties, while connection characteristics play a secondary role.

5.2. Multi-objective optimisation

Fig. 13 illustrates the results of the multi-objective optimisation process applied to RWS connections, considering seven mechanical performance criteria—Yield Moment, Maximum Moment, Ultimate Moment, Dissipated Energy, Equivalent Viscous Damping, Ductility Under Sagging, and Ductility Under Hogging—along with total embodied carbon (EC) reduction as a sustainability objective. The figure presents a pairwise correlation matrix between these variables, showing the trade-offs and interactions between different performance metrics.

The scatter plots compare the optimized solutions (red) with the real dataset (blue), providing insights into the feasible design space and the diversity of the Pareto-optimal solutions. Notably, strong positive correlations are observed among Yield Moment, Maximum Moment, and Ultimate Moment, indicating that increasing the flexural strength of RWS connections tends to improve all three moment capacities simultaneously. However, trade-offs emerge between mechanical performance and sustainability objectives, where higher structural strength may result in an increase in embodied carbon, highlighting the necessity of balancing performance with environmental impact.

For Dissipated Energy and Equivalent Viscous Damping, the results suggest a nonlinear relationship with other structural properties, reinforcing the complexity of energy dissipation mechanisms in RWS connections. The distributions of Ductility Under Sagging and Ductility Under Hogging indicate that higher ductility values are generally associated with increased energy dissipation but may also contribute to greater embodied carbon, presenting a critical design trade-off.

It is worth noting that, a direct comparison with traditional RWS design formulas is limited, as such methods generally predict a single property (e.g., moment capacity). In contrast, the proposed framework simultaneously predicts eight properties and incorporates multi-objective optimisation, enabling a broader and more integrated design capability.

The Pareto-optimal solutions generated by NSGA-II provide a well-distributed set of optimized designs, enabling decision-makers to select optimal configurations based on structural performance priorities and sustainability constraints. These results underscore the effectiveness of the multi-objective optimisation framework in guiding the design of RWS connections, offering valuable insights into the interplay between mechanical properties and carbon footprint reduction. The Pareto-optimal solutions are directly integrated in the user-friendly online interface.

5.4. User-friendly interface

A user-friendly interface was developed and deployed online via Hugging Face at the following link (https://huggingface.co/spaces/MohamedRabie26/RWS_connections). This tool provides users with two functionalities: (1) Predictions based on user-defined input parameters and (2) Multi-objective optimisation, where users can specify one objective output, and the tool returns the corresponding optimal input parameters along with the six remaining mechanical properties and the total embodied carbon (EC) reduction. The optimization is based on the nearest Pareto-optimal solution generated from the multi-objective optimization process, ensuring that the suggested design configurations maintain a balance between performance and sustainability. The predictions are generated using the optimal ML model identified in this study, ensuring high accuracy and reliability. The interface includes an intuitive slider-based input system, allowing users to select values within the trained data range specified in Table 2, ensuring the generated outputs remain within the model's predictive capabilities for reliability and practicality. Additionally, the tool provides Pareto-optimal solutions, offering valuable insights into the trade-offs between different performance metrics and sustainability objectives, as illustrated in Fig. 14. The developed interface is intended for interpolative use within the parameter space of the training data, ensuring reliable predictions for configurations represented in the database. It is worth mentioning that predictions outside this range may carry higher uncertainty and are beyond the tool's intended scope.

Furthermore, this tool can be integrated into ML workflows via the Hugging Face API, facilitating its application in structural engineering optimization and sustainable design initiatives. This capability supports researchers and industry professionals in making data-driven decisions, enhancing the design efficiency of RWS connections, and promoting the development of structurally optimized and environmentally sustainable solutions.

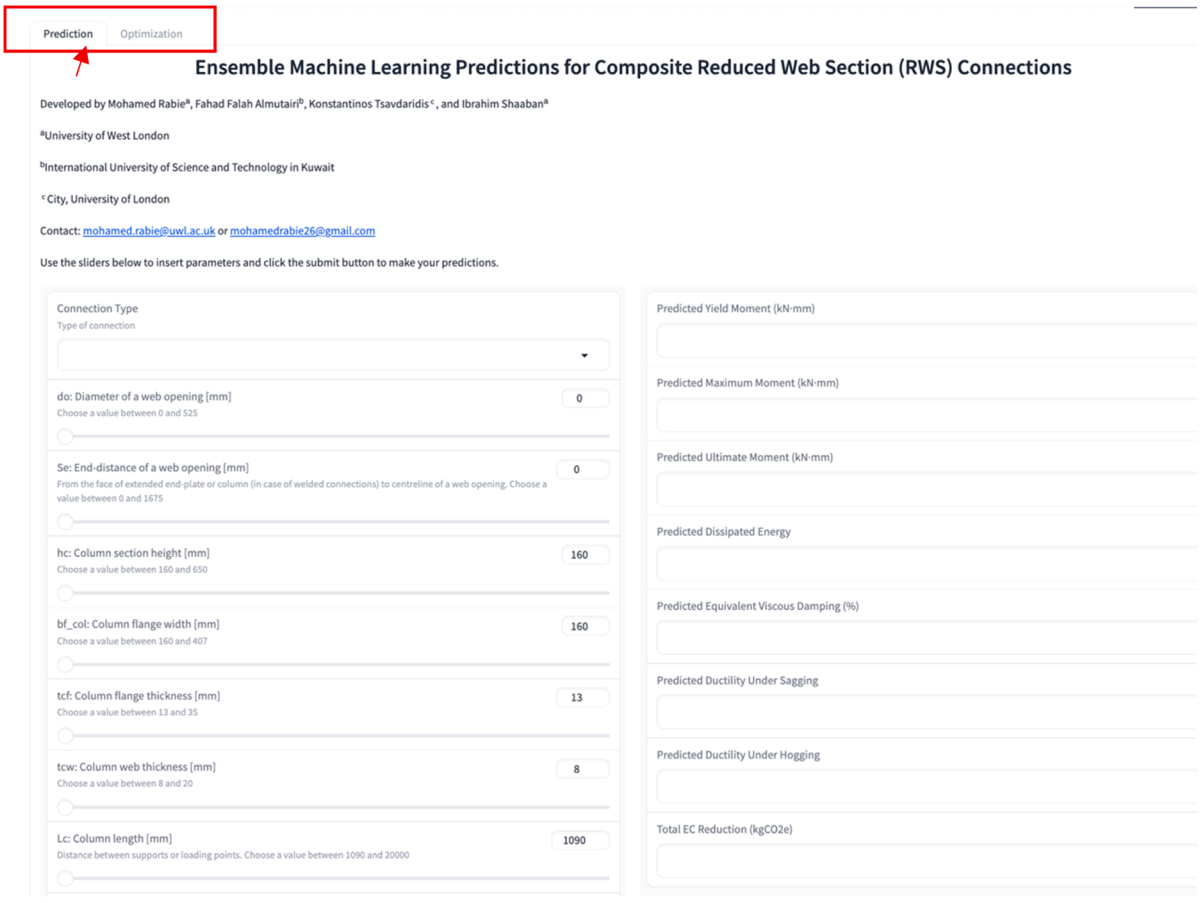

(a)

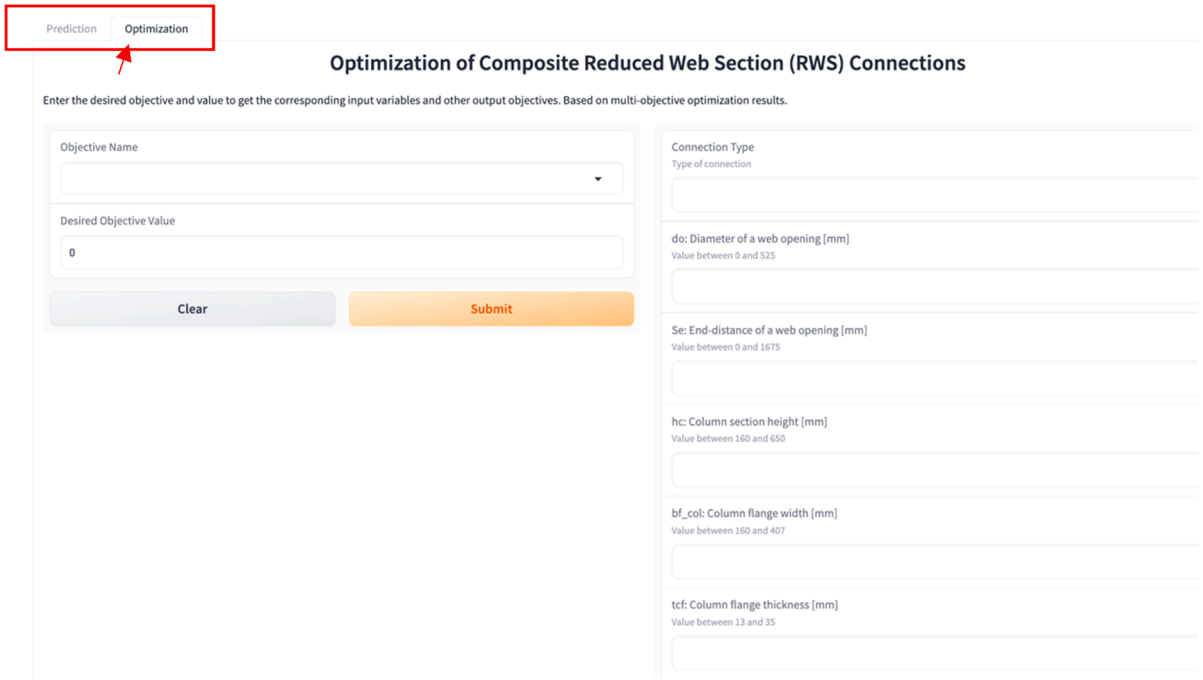

(b)

Fig. 14. Composite RWS connection online interface; (a) Mechanical and ductility properties prediction; (b) Multi-objective optimisation with for the output variables and corresponding input variables.

6. Concluding remarks

This study developed a machine learning-based framework for predicting and optimizing the mechanical performance and embodied carbon reduction of RWS connections. Three ensemble models namely, Extra Trees Regressor (ETR), Gradient Tree Boosting (GTBR), and Extreme Gradient Boosting (XGBoost) were evaluated, with XGBoost demonstrating superior generalization across most outputs. The SHAP analysis provided interpretability, confirming that key structural parameters, such as cross-sectional properties, material stiffness, and connection type, significantly influence the predicted responses. A multi-objective optimisation approach using NSGA-II was implemented to explore trade-offs between mechanical performance and embodied carbon reduction, generating Pareto-optimal solutions for informed decision-making.

The key findings are:

- Machine learning predictions confirmed that XGBoost consistently achieved the highest generalization performance, particularly for Yield Moment, Maximum Moment, and Ductility predictions, with the lowest test MAPE and highest R^2.
- SHAP analysis revealed that cross-sectional properties, particularly flange thickness (t_{bf}), cross-sectional area (A_a), and beam height (h_b), were the most influential features for predicting moment capacities.
- Ductility predictions were primarily governed by material properties and member stiffness, with concrete compressive strength (f_c), beam length (L_b), and column elastic modulus (E_{column}) playing a dominant role in both sagging and hogging ductility.
- Multi-objective optimization highlighted trade-offs between structural performance and sustainability, demonstrating that higher moment capacities and ductility often come at the cost of increased embodied carbon, requiring a balance in design selection.

Additionally, a user-friendly interface was developed and deployed on Hugging Face, enabling users to make predictions and retrieve optimized design parameters based on the nearest Pareto-optimal solutions. This tool facilitates efficient and sustainable design exploration by balancing structural performance and environmental impact, though it is intended specifically for preliminary design guidance and must be utilized alongside official structural standards for final practical verification. The findings demonstrate the potential of AI-driven decision support systems in structural engineering, paving the way for more data-driven, optimized, and sustainable connection designs.

Author agreement statement

We the undersigned declare that this manuscript is original, has not been published before and is not currently being considered for publication elsewhere.

We confirm that the manuscript has been read and approved by all named authors and that there are no other persons who satisfied the criteria for authorship but are not listed. We further confirm that the order of authors listed in the manuscript has been approved by all of us.

We understand that the Corresponding Author is the sole contact for the Editorial process. He/she is responsible for communicating with the other authors about progress, submissions of revisions and final approval of proofs

Data availability statement

The compiled database of RWS connections is openly available in a public repository to facilitate reproducibility and further research (Mendeley Data, https://data.mendeley.com/datasets/66s35tgvd3/1).

CRediT authorship contribution statement

Mohamed Rabie: Writing – original draft, Visualization, Software, Investigation, Formal analysis, Data curation. **Fahad Falah Almutairi:** Writing – review & editing, Visualization, Software, Methodology, Formal analysis, Data curation. **Konstantinos Daniel Tsavdaridis:** Writing – review & editing, Validation, Supervision, Software, Methodology, Investigation, Conceptualization. **Ibrahim G. Shaaban:** Writing – review & editing, Supervision, Project administration, Funding acquisition.

Declaration of competing interest

The authors declare that they have no known competing financial interests or personal relationships that could have appeared to influence the work reported in this paper.

Acknowledgements

This work was partially funded by the University of West London Vice Chancellor's Scholarship awarded to the first author.

References

[1] Uang C-M, Kent" Yu Q-S, Noel S, Gross J. Cyclic testing of steel moment connections rehabilitated with RBS or welded haunch. J. Struct. Eng. 2000;126:57–68.
[2] X. Zhang, J.M. Ricles, L.-W. Lu, J.W. Fisher, Development of seismic guidelines for deep-column steel moment connections, (2004).
[3] D'Aniello M, Tartaglia R, Landolfo R, Jaspart J-P, Demonceau J-F. Seismic pre-qualification tests of EC8-compliant external extended stiffened end-plate beam-to-column joints. Eng. Struct. 2023;291:116386.
[4] AISC, China, Global warming and hot-rolled structural Steel sections., American Steel Institute, white paper F157-18., 2018.
[5] Mullholland A, Ackerman C, Astle P, Drewniok M, Dunster A, Hibbert A, Inman R, Kershaw R, Martin B, McCague C. Low carbon concrete routemap. Setting the Agenda for a Path to Net Zero 2022.
[6] Almutairi FF, Tsavdaridis KD. Capacity design assessment of composite reduced web section (RWS) connections. Eng. Struct. 2024;316:118558. https://doi.org/10.1016/j.engstruct.2024.118558.
[7] Erfani S, Akrami V. Increasing seismic energy dissipation of steel moment frames using reduced web section (RWS) connection. J. Earthq. Eng. 2017;21:1090–112.
[8] Almutairi FF, Tsavdaridis KD, Alonso-Rodriguez A, Hajirasouliha I. Experimental investigation using demountable steel-concrete composite reduced web section (RWS) connections under cyclic loads. Bull. Earthq. Eng. 2024;22:1081–110. https://doi.org/10.1007/s10518-023-01802-y.
[9] Lin S, Qiao H, Wang J, Shi J, Chen Y. Anti-collapse performance of steel frames with RWS connections under a column removal scenario. Eng. Struct. 2021;227:111495.
[10] Tsavdaridis KD, Lau CK, Alonso-Rodríguez A. Experimental behaviour of non-seismical RWS connections with perforated beams under cyclic actions. J. Constr. Steel Res. 2021;183:106756.
[11] Nazaralizadeh H, Ronagh H, Memarzadeh P, Behnamfar F. Cyclic performance of bolted end-plate RWS connection with vertical-slits. J. Constr. Steel Res. 2020;173:106236.
[12] Tsavdaridis KD, D'Mello C. Vierendeel bending study of perforated steel beams with various novel web opening shapes through nonlinear finite-element analyses. J. Struct. Eng. 2012;138:1214–30.
[13] Tsavdaridis KD, Faghih F, Nikitas N. Assessment of perforated steel beam-to-column connections subjected to cyclic loading. J. Earthq. Eng. 2014;18:1302–25.
[14] Akrami V, Erfani S. Effect of local web buckling on the cyclic behavior of reduced web beam sections (RWBS). Steel Compos. Struct. 2015;18:641–57.
[15] Tsavdaridis KD, Pilbin C, Lau CK. FE parametric study of RWS/WUF-B moment connections with elliptically-based beam web openings under monotonic and cyclic loading. Int. J. Steel Struct. 2017;17:677–94.
[16] Erfani S, Akrami V, Mohammad-nejad A. Lateral load resisting behavior of steel moment frames with reduced web section (RWS) beams, in: structures. Elsevier; 2020. p. 251–65.
[17] Erfani S, Akrami V. A nonlinear macro-model for numerical simulation of perforated steel beams. Int. J. Steel Struct. 2019:1–19.
[18] Boushehri K, Tsavdaridis KD, Cai G. Seismic behaviour of RWS moment connections to deep columns with European sections. J. Constr. Steel Res. 2019;161:416–35.
[19] Shaheen MA, Tsavdaridis KD, Yamada S. Comprehensive FE study of the hysteretic behaviour of steel-concrete composite and non-composite RWS beam-to-column connections. J. Struct. Eng. 2018.
[20] Almutairi FF, Tsavdaridis KD, Rodriguez AAlonso, Asteris PG, Lemonis ME. Hysteretic behaviour of composite reduced web section (RWS) connections for

seismic applications. J. Earthq. Eng. 2023;28:349–84. https://doi.org/10.1080/13632469.2023.2204172.
[21] Tabar AM, Alonso-Rodriguez A, Daniel Tsavdaridis K. Building retrofit with reduced web (RWS) and beam (RBS) section limited-ductility connections. J. Constr. Steel Res. 2022.
[22] Khoshkroodi A, Sani HP, Aajami M. Stacking ensemble-based machine learning model for predicting deterioration components of steel W-section beams. Buildings 2024. https://doi.org/10.3390/buildings14010240.
[23] Cheng K, Lu Z. Structural reliability analysis based on ensemble learning of surrogate models. Struct. Saf. 2020. https://doi.org/10.1016/j.strusafe.2019.101905.
[24] Hamburger RO, Malley JO. Seismic design of steel special moment frames. US Department of Commerce, National Institute of Standards and Technology …; 2016.
[25] Georgiou G, Elkady A. ANN-based model for predicting the nonlinear response of flush endplate connections. J. Struct. Eng. 2024;150:4024034.
[26] Ferreira FPV, Shamass R, Limbachiya V, Tsavdaridis KD, Martins CH. Lateral–torsional buckling resistance prediction model for steel cellular beams generated by Artificial Neural Networks (ANN). Thin-Walled Struct. 2022;170:108592.
[27] Degtyarev VV, Tsavdaridis KD. Buckling and ultimate load prediction models for perforated steel beams using machine learning algorithms. J. Build. Eng. 2022;51:104316.
[28] Rabie M, Shaaban IG. Glass fibre concrete: experimental investigation and predictive modeling using advanced machine learning with an interactive online interface. Constr. Build. Mater. 2025;472:140951. https://doi.org/10.1016/j.conbuildmat.2025.140951.
[29] Wakjira TG, Ibrahim M, Ebead U, Alam MS. Explainable machine learning model and reliability analysis for flexural capacity prediction of RC beams strengthened in flexure with FRCM. Eng. Struct. 2022;255:113903. https://doi.org/10.1016/j.engstruct.2022.113903.
[30] Wakjira TG, Kutty AA, Alam MS. A novel framework for developing environmentally sustainable and cost-effective ultra-high-performance concrete (UHPC) using advanced machine learning and multi-objective optimization techniques. Constr. Build. Mater. 2024;416:135114. https://doi.org/10.1016/j.conbuildmat.2024.135114.
[31] Wakjira TG, Alam MS. Peak and ultimate stress-strain model of confined ultra-high-performance concrete (UHPC) using hybrid machine learning model with conditional tabular generative adversarial network. Appl. Soft Comput. 2024;154:111353. https://doi.org/10.1016/j.asoc.2024.111353.
[32] Li C, Li H, Chen X. A framework for fast estimation of structural seismic responses using ensemble machine learning model. Smart Struct. Syst. 2021;28:425–41.
[33] Vlasenko T, Hutsol T, Vlasovets V, Glowacki S, Nurek T, Horetska I, Kukharets S, Firman Y, Bilovod O. Ensemble learning based sustainable approach to rebuilding metal structures prediction. Sci. Rep. 2025;15:1210.
[34] Molnar C. Interpretable machine learning. Lulu. com 2020.
[35] Lundberg SM, Lee S-I. A unified approach to interpreting model predictions. Adv. Neural Inf. Process. Syst. 2017;30.
[36] Loyola-González O. Black-Box vs. White-Box: understanding their advantages and weaknesses from a practical point of view. IEEE Access 2019;7:154096–113. https://doi.org/10.1109/ACCESS.2019.2949286.
[37] Tingley DD, Davison B. Developing an LCA methodology to account for the environmental benefits of design for deconstruction. Build. Environ. 2012;57:387–95.
[38] Akinade OO, Oyedele LO, Ajayi SO, Bilal M, Alaka HA, Owolabi HA, Bello SA, Jaiyeoba BE, Kadiri KO. Design for deconstruction (DfD): critical success factors for diverting end-of-life waste from landfills. Waste Manag. 2017;60:3–13.
[39] Guo B, Wang JT, Liang T, Bao Z. Study on seismic performance of a new type energy dissipation steel moment frames. In: Appl. Mech. Mater., Trans Tech Publ; 2011. p. 764–70.
[40] Li B, Yang Q, Yang N. An investigation on aseismic connection with opening in beam web in steel moment frames. Adv. Struct. Eng. 2011;14:575–87.
[41] Tsavdaridis KD, Papadopoulos T. A FE parametric study of RWS beam-to-column bolted connections with cellular beams. J. Constr. Steel Res. 2016;116:92–113.
[42] Shin M, Kim S-P, Halterman A, Aschheim M. Seismic toughness and failure mechanisms of reduced web-section beams: phase 2 tests. Eng. Struct. 2017;141:607–23.
[43] Zhang X, Zheng S, Zhao X. Seismic performance of steel beam-to-column moment connections with different structural forms. J. Constr. Steel Res. 2019;158:130–42.
[44] Xu Q, Chen H, Li W, Zheng S, Zhang X. Experimental investigation on seismic behavior of steel welded connections considering the influence of structural forms. Eng. Fail. Anal. 2022;139:106499.
[45] Nguyen MH, Mai H-VT, Trinh SH, Ly H-B. A comparative assessment of tree-based predictive models to estimate geopolymer concrete compressive strength. Neural Comput. Appl. 2023;35:6569–88. https://doi.org/10.1007/s00521-022-08042-2.
[46] Sharma U, Gupta N, Verma M. Prediction of compressive strength of GGBFS and Flyash-based geopolymer composite by linear regression, lasso regression, and ridge regression. Asian J. Civ. Eng. 2023;24:3399–411. https://doi.org/10.1007/s42107-023-00721-2.
[47] Anjum M, Khan K, Ahmad W, Ahmad A, Amin MN, Nafees A. Application of ensemble machine learning methods to estimate the compressive strength of Fiber-reinforced nano-silica modified concrete. Polymers (Basel) 2022;14:3906. https://doi.org/10.3390/polym14183906.
[48] Rana MS, Hossain MM, Li F. Comparative analysis of machine learning models for predicting the compressive strength of ultra-high-performance steel fiber reinforced concrete. J. Eng. Res. 2025. https://doi.org/10.1016/j.jer.2025.01.004.
[49] Rabie M, Ibrahim M, Ebead U, Shaaban IG. Optimising sustainable alkali-activated mortar: experimental work and machine learning predictions. Proc. Inst. Civ. Eng. - Struct. Build. 2025;178:828–50. https://doi.org/10.1680/jstbu.25.00036.
[50] Geurts P, Ernst D, Wehenkel L. Extremely randomized trees. Mach. Learn. 2006;63:3–42.
[51] D. Kocev, M. Ceci, Ensembles of extremely randomized trees for multi-target regression, (2015) 86–100. https://doi.org/10.1007/978-3-319-24282-8_9.
[52] Hastie T, Tibshirani R, Friedman J. The elements of statistical learning. New York, NY: Springer; 2009. https://doi.org/10.1007/978-0-387-84858-7.
[53] Friedman JH. Greedy function approximation: a gradient boosting machine. Ann. Stat. 2001:1189–232.
[54] Chen T, Guestrin C. XGBoost: A scalable tree boosting system. In: Proc. 22nd ACM SIGKDD Int. Conf. Knowl. Discov. Data Min; 2016. p. 785–94. https://doi.org/10.1145/2939672.2939785.
[55] Hastie T, Tibshirani R, Friedman J. Ensemble Learning. Eds.. In: Hastie T, Tibshirani R, Friedman J, editors. Elem. Stat. Learn. Data Min. Inference Predict. New York, NY: Springer; 2009. p. 605–24. https://doi.org/10.1007/978-0-387-84858-7_16.
[56] Cakiroglu C, Shahjalal M, Islam K, Mahmood SMF, Billah AHMM, Nehdi ML. Explainable ensemble learning data-driven modeling of mechanical properties of fiber-reinforced rubberized recycled aggregate concrete. J. Build. Eng. 2023;76:107279. https://doi.org/10.1016/J.JOBE.2023.107279.
[57] Deb K, Pratap A, Agarwal S, Meyarivan T. A fast and elitist multiobjective genetic algorithm: NSGA-II. IEEE Trans. Evol. Comput. 2002;6:182–97. https://doi.org/10.1109/4235.996017.
[58] Orr J, Gibbons O, Arnold W. A brief guide to calculating embodied carbon. Struct. Eng. 2020;98:22–7. https://doi.org/10.56330/JZNX5709.
[59] British Steel, Environmental product declaration (EPD) report of steel rails and sections (including semi-finished long products), BRC Limited, Gwent, 2020. https://britishsteel.co.uk/who-we-are/sustainability/.
[60] S.E.P. Book, A brief guide to calculating embodied carbon, (n.d.).
[61] Rabie M, Irshidat MR, Al-Nuaimi N. Ambient and heat-Cured Geopolymer composites: mix design optimization and life cycle assessment. Sustainability 2022;14:4942.
[62] Irshidat MR, Al-Nuaimi N, Ahmed W, Rabie M. Feasibility of recycling waste carbon black in cement mortar production: environmental life cycle assessment and performance evaluation. Constr. Build. Mater. 2021;296:123740.
[63] Akiba T, Sano S, Yanase T, Ohta T, Koyama M. Optuna: A next-generation hyperparameter optimization framework. In: Proc. 25th ACM SIGKDD Int. Conf. Knowl. Discov. Data Min; 2019.
[64] Curtis LE, Murray TM. Column flange strength at moment end-plate connections. Eng. J. 1989;26:41–50.
[65] Elhout EA. Effect of beam-column connection types on the response modification factors of steel frames. Int. J. Steel Struct. 2024;24:132–43. https://doi.org/10.1007/s13296-023-00805-4.
[66] Rodgers JE, Mahin SA. Effects of connection deformation softening on behavior of steel moment frames subjected to earthquakes. Int. J. Steel Struct. 2011;11:29–37. https://doi.org/10.1007/S13296-011-1003-9.
[67] Joshi JR, Huang J. Numerical study of HSS-to-HSS moment connections subjected to out-of-plane loading: effect of connection eccentricity. Int. J. Civ. Infrastruct. 2023;6:51–7.
[68] Jiao Y, Yamada S, Kishiki S, Shimada Y. Evaluation of plastic energy dissipation capacity of steel beams suffering ductile fracture under various loading histories. Earthq. Eng. Struct. Dyn. 2011;40:1553–70. https://doi.org/10.1002/eqe.1103.
[69] Yu Y-S, Liu X-Y. Finite element analyses on energy dissipation capacity of upper flange welded-lower flange bolted beam-column connection with slotted holes. J. Asian Archit. Build. Eng. 2020;19:315–26. https://doi.org/10.1080/13467581.2020.1749639.
[70] Liu T, Chen S, Feng Z, Liu H. Effect of web openings on flexural behaviour of underground metro station RC beams under static and cyclic loading. Adv. Civ. Eng. 2020;2020:1210485. https://doi.org/10.1155/2020/1210485.
[71] Cai J, Deng Z, Li W. Numerical study on seismic behavior of demountable joints consisting of reinforced concrete columns and steel beams. Buildings 2023;13:2558. https://doi.org/10.3390/buildings13102558.
[72] Tsavdaridis KD, Papadopoulos T. A FE parametric study of RWS beam-to-column bolted connections with cellular beams. J. Constr. Steel Res. 2016;116:92–113. https://doi.org/10.1016/j.jcsr.2015.08.046.
[73] Sarfarazi S, Shamass R, Guarracino F, Mascolo I, Modano M. Exploring the stainless-steel beam-to-column connections response: A hybrid explainable machine learning framework for characterization. Front. Struct. Civ. Eng. 2025;19:34–59. https://doi.org/10.1007/s11709-025-1162-y.